NTNU

Norwegian University of
Science and Technology

Impact of EV Integration and Fast Chargers in a Norwegian LV Grid

An analysis based on data from a residential
grid in Steinkjer

Martin Lillebo

Master of Energy and Environmental Engineering
Submission date: January 2018
Supervisor: Hossein Farahmand, IEL
Co-supervisor: Salman Zaferanlouei, IEL
Antonio Zecchino, DTU, Dept. of Electrical Engineering

Norwegian University of Science and Technology
Department of Electric Power Engineering

NTNU

Norwegian University of
Science and Technology

Impact of EV Integration and Fast Chargers in a Norwegian LV Grid

An analysis based on data from a distribution grid in Steinkjer

Martin Lillebo

Master of Energy and Environmental Engineering

Submission date: January 2018

Supervisor: Hossein Farahmand, NTNU, IEL
Co-supervisors: Salman Zaferanlouei, NTNU, IEL
Antonio Zecchino, DTU, Dept. of Electrical Engineering

Norwegian University of Science and Technology
Department of Electric Power Engineering

Acknowledgements

This master's thesis is written at the Department of Electric Power Engineering at the Norwegian University of Science and Technology. It was written during the fall semester in 2017 and a few weeks in January 2018, and marks my conclusion of the MSc programme in Energy and Environmental Engineering.

I want to thank my supervisor, Hossein Farahmand, for giving me guidance throughout the semester and freedom to take the thesis in the directions I wanted. I am also very grateful for the help and motivation I have gotten from my co-supervisors, Salman Zaferanlouei and Antonio Zecchino.

Finally, I want to thank my friends, family and girlfriend, all of whom I am very lucky to have in my life.

Trondheim, January 2018

Martin Lillebo

Abstract

Given a renewable power supply, the replacement of conventional vehicles with electric alternatives has the potential to significantly reduce climate gas emissions from the transport sector. Norway has implemented economic incentives over several years to encourage a transition from conventional vehicles to electric cars (EVs), and has now the largest share of EVs per capita in the world. The power levels required to charge this fleet may constitute a significant strain on the existing power grid, especially at a low voltage level. The deployment of fast chargers may further aggravate this. More knowledge about the challenges ahead will be advantageous.

This thesis explores the effects of increasing EV penetration levels in a Norwegian distribution grid, by analyzing real power measurements obtained from household smart meters. The implications of installing a fast charger in the grid has been assessed, an optimal location for it has been proposed, and the potential for reactive power injection to reduce the voltage deviations caused by it has been investigated.

After presenting the theoretical groundwork, data set and methodology, the model is presented in detail and the following results are described. Results show that the EV hosting capacity of the grid is good for a majority of the end-users, but that the weakest power cable would be overloaded at a 20 % EV penetration level. The network tolerated an EV penetration of 50 % with regards to the voltage levels at all end-users. Injecting reactive power at the location of an installed fast charger proved to significantly reduce the voltage deviation otherwise imposed by the charger.

Sammendrag

Med utgangspunkt i en fornybar kraftforsyning, vil utfasingen av konvensjonelle kjøretøy til fordel for elektriske kjøretøy ha et stort potensial for å redusere klimagassutslipp knyttet til transportsektoren. Norge har implementert økonomiske insentiver over flere år for å oppmuntre til en overgang til elbiler, og har nå verdens største andel av elbiler per innbygger. Effektnivåene som kreves for å lade denne elektriske bilflåten kan vise seg å være en betydelig belastning på det eksisterende kraftnettet, spesielt på lavspent nivå. Utbyggingen av hurtigladere kan forverre dette ytterligere. Det er derfor ønskelig med økt kunnskap om disse utfordringene.

Denne masteroppgaven utforsker effekten av en økende andel elbiler i et norsk fordelingsnett, ved å analysere ekte måledata fra smartmålere i husholdninger lokalisert i Steinkjer. Implikasjonene av å installere en hurtiglader i det samme nettet har blitt vurdert, en optimal plassering av den er blitt foreslått, og potensialet for å benytte reaktiv fasekompensering for å redusere spenningsfall tilknyttet bruk av ladepunktet har blitt undersøkt.

Etter å ha presentert et teoretisk grunnlag, datasettet og den benyttede metoden, er modellen blitt beskrevet i detalj og studiets resultater er blitt lagt frem. Resultatene viser at tilknytningskapasiteten for elbiler er god for en majoritet av sluttbrukerne, men at den svakeste jordledningen ble overbelastet ved en elbilandel på 20 %. Med hensyn til nettspenningen tålte alle sluttbrukere i nettet en elbilandel på 50 % før spenningen på et punkt falt under grensen 10 % av nominell verdi. Ved å injisere reaktiv effekt ved lokasjonen til en installert hurtiglader, viste modellen at spenningsavviket som ellers ville oppstått ved bruk av laderen ble betydelig redusert.

Contents

List of Figures

List of Tables

Abbreviations

DSB	Norwegian Directorate for Civil Protection
DSO	Distribution System Operator
EV	Electric vehicle
FC	Fast charger
mpc	MATPOWER case struct
NTE	Nord-Trøndelag Elektrisitetsverk
NEVA	Norwegian EV Association
NVE	Norwegian Water Resource and Energy Directorate
PF	Power factor

1 Introduction

1.1 Problem description and motivation

Electric vehicles (EVs) have grown significantly in interest. When driven on electricity with a low carbon footprint, they cause less greenhouse gas emissions over the course of their life cycle [1]. Viewed as an effective measure to reduce the climate impact of the transport sector, governments around the world have initiated policies to encourage consumers to drive electric. Norway's economic incentives have been particularly effective, and Norway has today the largest share of EVs per capita in the world [2].

The electrical energy required to fuel an increasingly more electrified transport sector in Norway is expected to constitute a tolerable addition to the existing consumption. By 2030, the Norwegian Water Resource and Energy Directorate (NVE) estimated that Norway may host 1.5 million EVs, which will require 4 TWh of electricity annually [3]. This is less than the estimated 6.5 TWh of new annual wind power capacity currently under construction in Norway by the end of 2017, and another 17.1 TWh of expected annual production has been granted approval to be constructed, mainly in the form of wind power [4]. The power levels required to charge this fleet may however constitute a significant strain on the existing power grid. The necessary power levels can be higher than the rated power capacities of the lines and transformers in the power grid. NVE calculated in 2016 that a an average power increase of 5 kW consumption in all households will overload more than 30 % of the distribution grid transformers in Norway [3]. It is therefore reason to believe that a large number of EVs charging simultaneously with similar power levels may cause overloading of grid components.

Public fast chargers are being built to strengthen the range and attractiveness of electric transportation. The potentially high amounts of power they can draw will pose an additional challenge to the grid, and a well-considered placement of the fast charging point will be valuable. If the voltage level drops too far, the charger may be able to offer a voltage-stabilizing service by injecting reactive power [5].

More knowledge about the extent of these coming challenges to power grid security will be advantageous for decision makers like distribution system operators (DSOs), as it will allow them to take a more proactive approach to potential infrastructure investments in the power grid. This knowledge can be acquired by analyzing the measured end-user power use, which stems from the smart meters currently being installed in Norway. By conducting load flow analyses with real measured energy use as input values, the power flow in all lines and voltage magnitudes at all buses can be calculated. This will provide the DSO with valuable information on whether a specific part of a power grid is capable of carrying the load from increased EV-charging or not.

1.2 Research questions

This thesis will contribute to better the knowledge of the distribution grids' current states, their EV hosting capacities and their response to potential fast charging. This will be done by conducting a series of load flow studies and subsequent analysis and assessments of the results.

The analyses will be based on a whole year of hourly active power flow measurements at all end-users, in a specific distribution grid located in Steinkjer, Norway. Specifically, this thesis aims to:

- Assess the current state of the grid, with respect to voltage levels and load ratios at buses/branches in the grid
- Assess the grid's EV hosting capacity, with respect to voltage levels and load ratios at buses/branches in the grid
- Choose a specific EV penetration as a base case, and assess the effects of including a 22 kVA fast charger in the grid
- Investigate the potential benefits of including reactive power control in the fast charger, thus allowing it to respond to and prevent unacceptable voltage deviations

1.3 Scope

- The distribution grid model will be based on active power consumption data and branch connection information from a 95-bus system in Steinkjer, Norway
- All power use measurements stems from data given by the DSO Nord-Trøndelag Elektrisitetsverk (NTE)
- The load flow studies will be conducted in MATPOWER, which assumes a balanced system at all times
- The EV-loads will be based on an EV charging profile derived from the smart meter measurements from a household which contains a regularly used EV
- The fast charger load profile will be modelled as a constant load, and will hence be a worst-case use case.
- The thesis will not analyze smart charging solutions, with the exception of reactive power control

1.4 Thesis contributions

- Conducts a thorough assessment of the EV hosting capacity of a Norwegian distribution grid, based on real measurement data
- Demonstrates an algorithm used to find the best grid connection point for a fast charger or similarly large load. It is done by minimizing the consequential voltage deviations in the system as a whole, while also considering the power losses in the grid
- Demonstrates the use of reactive power injection to reduce voltage deviations in the network

1.5 Thesis structure

Chapter 1 includes motivation and problem description, the research question, scope and contributions made in this thesis

Chapter 2 goes through relevant literature on the topic of challenges posed by EV charging on low-voltage grids and the importance of meeting these, before giving the reader a summary of the state of the current EV fleet in Norway and their typical modes of charging. The basic theory underlying reactive power is introduced, as well as the concept of reactive power control as a measure to stabilize voltage drops. An introduction to load flow studies is then given, before the MATPOWER software package is described

Chapter 3 describes the distritribution grid in Steinkjer which will be the basis of this study, including specifics on the information given by the DSO and the data derived from it

Chapter 4 deals with the specifics on how the load flow model was built, run, and how data was collected from it afterwards

Chapters 5 to 7 contain the results for all different cases

Chapter 8 discusses the main elements from the results, including the first simulation of the un-edited grid, the EV charging graph, the EV hosting capacity of the grid, and the various implementations of the fast charger and its implications.

Chapter 9 contains concluding remarks

Chapter 10 contains suggestions for further work.

2 Theory

2.1 Historical EV development in Norway

As seen in Figure 2.1, by the end of 2017 the EV market share in the private car sector in Norway rose to 20 %, and it was registered more than 135 000 EVs in the country. More than 65 000 plug-in hybrid cars come in addition to these [6]. With a total passenger car fleet of 2 662 910 vehicles at the end of 2017, the share of full-electric EVs approximates to 5.4 % of all passenger cars in the country [7]. This has made Norway the country in the world with the highest number of EVs per capita [2].

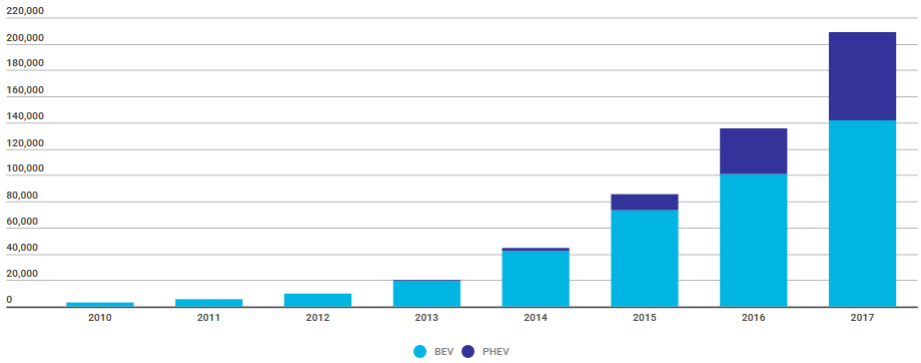

Figure 2.1: Historical development of cumulative amount of EVs registered in Norway [6]

2.2 IT and TN grids

There are two main types of distribution voltage systems in Norway: IT (french: "Isolée Terre") and TN (Terra Neutral) grids. Power for a common 230 V single phase load is drawn from an IT grid by by connecting two of the 230 V phases together, while the TN grid provides the same voltage by connecting the load between one of its 400 V phases and a neutral line, resulting in 230 V. More than 70 % of the Norwegian distribution grid is built as an IT-grid, which with the exception of Albania is a grid topology that is unique in Europe [8]. As an IT-grid usually only allows single phase power consumption, the maximal available power is effectively limited to 7.3 kW. This is due to the nominal voltage of 230 V and a maximal allowed current through one phase of 32 A [8].

2.2.1 Standard outlet

The common household plug in Norway is often called the *Schuko*-plug, which stems from the German word *Schutzkontakt - protection plug*. It is usually fitted for 10 A or 16 A currents, allowing up to 3,7 kW charging in an IT-grid. Although able to carry these currents, it is not designed to withstand a max rated current being drawn for several hours every day. Periodic EV-charging from a Schuko outlet is therefore decided by Norwegian law to be max 10 A, and The Norwegian Directorate for Civil Protection (DSB) recommends to further reduce this down to 8 A as [9].

2.3 Charging modes

The charging mode denotes the technology used to charge the EV, and ranges from mode 1 to mode 4. The difference between these are outlined in the paragraphs below.

Mode 1 is the connection to the vehicle through a standard grounded outlet, also called the Schuko outlet The maximum allowed current through a Schuko outlet is 16 A, allowing a charge rate of 3,7 kW.

Mode 2 denotes a connection to the standard Schuko outlet using a special cable that includes a control module between the outlet and the EV. This module contains earth fault protection and communication software for signaling the car about whether the connection is secure, and to limit the current drawn from the grid. Max 32 A is drawn through the one phase or three phase grid connection, given that the circuitry to which it is connected is sufficiently rated for current that high. The Norwegian Directorate for Civil Protection recommends standard outlets used for periodic EV-charging to be limited to max 10 A, due to the long periods of use involved and the accompanying risk for overheating [9]. Most EVs today come with a mode 2 charger included. Although it is primarily meant to be used as the charger cable when travelling and parking at locations where the Schuko outlet is the only option, although the majority of EV owners - approx. 63 % - use it as the main household charging solution. [10]

Mode 3 charging implies a dedicated stationary charging station. Charging communication, supervisory functions and earth fault protection is included inside the station. This is the recommended household charging solution for EV owners, and approx. 31 % of Norwegian EV owners has a mode 3 charger installed in their household [10].

Mode 4 charging is the charging infrastructure used for DC fast charging found in the Japanese CHAdeMO, the European CCS and the Tesla Supercharger standards. By charging directly with DC current, the charging current is no longer limited by the built-in inverter inside the EV, thus allowing higher currents. The CHAdeMO standard is most often limited to 50 kW, CCS is limited to 86 kW and the Tesla Supercharger allows charging up to 135 kW [11].

2.4 EV load profiles

The power drawn to charge an EV may effectively double or triple a given household's power use during the time of charging. This is illustrated in an excerpt of 8 days of hourly smart meter measurements of two households, shown in Figure 2.2. The power series with the largest peak values stems from an end-user who is confirmed to charge an EV with 7.3 kW charger. The other series belongs to an end-user with a comparable base load profile, but without EV-charging. The five largest peaks all happen between 18:00 and 21:00.

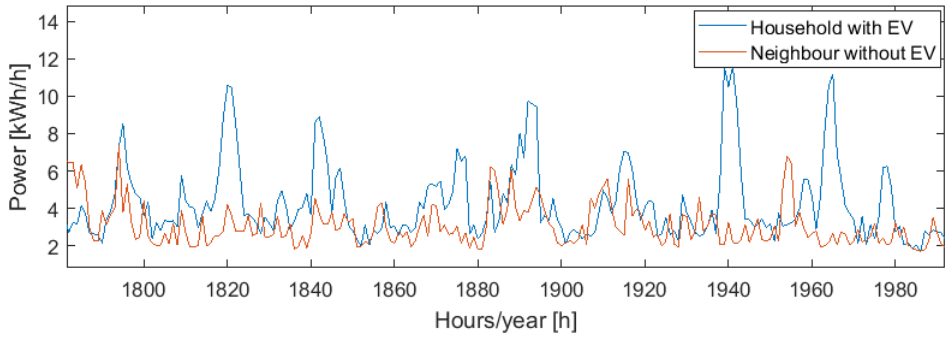

Figure 2.2: A comparison between two households, one of which regularly charges an EV. The 5 largest power peaks occur between 18:00 and 21:00

There is little available data on EV charging patterns spanning over larger periods of time. When assessing the impact of EV charging on the Norwegian power grid, NVE used charging measurements conducted by SINTEF, the longest one spanning 12 weeks [3].

The Norwegian Electric Vehicle Association (NEVA) has gathered data on which type of charging most households have chosen for their EVs. A survey was sent to NEVAs members base in 2017, and 12 510 replies was collected. 63 % replied they only use a regular Schuko-outlet for charging, either directly or with a mode 2 charging cable. This limits the power output to 2.3 kW in an IT-grid. 31 % had a dedicated mode 3 charger, allowing a charging current of either 16 A or 32 A, giving 3.7 kW or 7.3 kW in an IT-grid, respectively.

2.5 EV hosting capacity

The EV hosting capacity is a measure of how large EV penetration the grid in question can hold before any set constraints are violated.

The grid to be analyzed in this thesis has previously had its EV hosting capacity assessed. In a Master's thesis conducted at NTNU, a larger grid in the same region,

including several IT-grids, had its EV hosting capacity assessed with the help of load flow studies. It was concluded that an EV penetration of 25 % with 32 A charging currents could cause voltage deviations larger than 0.1 p.u. in parts of the IT-grids in the network. It was added that smart charging regimes to shift the load off-peak and limiting the charging current to 16 A could elevate this to 100 % [12]. The study assumed a self-constructed EV charging pattern and based the household consumption profiles on a calculated average from 8 houses.

A thesis from 2012 conducted a similar assessment of a nearby grid about 1/3 of the size of the one assessed in this study [13], with an approximately equally high peak power consumption rate (6 kW vs. 7.3 kW in this study), where it was concluded that the grid could not handle an EV-share of 60 % unless co-ordinated smart charging was implemented. However, no EV penetration between 10 % and 60 % was investigated in that study.

2.6 Reactive power control

The reactive power flow in the network can to an extent be manipulated in order to stabilize the voltage level. The following subchapter will give an introduction to the concept of reactive power, and describe how it can be controlled in order to reduce potential voltage drops in the system.

2.6.1 Reactive power

Reactive power plays an important part in electrical power systems. The power cables' power capacity is not only occupied by the real power demand that is consumed in the load. A certain amount of energy is not consumed, but temporarily stored and returned through the same line during the next part of the alternating current cycle. Although not consumed, this reactive power, Q, occupies its share of the nominal transfer capacity of the lines or cables involved. The presence of Q is the result of a mismatch between the current and voltage phase angles, as displayed in Figure 2.4(a).

The power factor $PF = \cos\phi = \frac{P}{S}$ is commonly used as a measurement of the degree to which the total apparent power S is constituted of active power P, where ϕ denotes the angle between the current phasor and the voltage phasor. The remaining parts of S is constituted of reactive power. The relationship is illustrated in Figure 2.3. By using the Pythagorean theorem, the following relationships can be derived:

$$|S| = \sqrt{P^2 + Q^2} \tag{2.1}$$

$$Q = P\tan\phi \tag{2.2}$$

where

$\|S\|$	Is the length of the vector S, which is the measured apparent power in a given cable

S can be expressed in its complex form $S = P + jQ$, while the actual length of the vector S, $|S| = \sqrt{P^2 + Q^2}$ gives us the apparent power flowing through the cable.

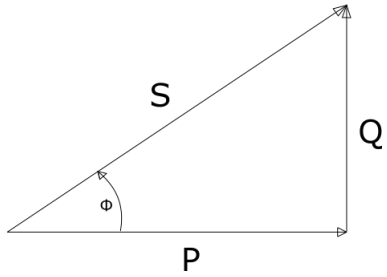

Figure 2.3: The vector sum of active and reactive power sums up to the apparent power, S

The product of V×I in Figure 2.4(a) will give the apparent power S, while P and Q can be found by multiplying together the active and reactive components (real and imaginary component) of the current and voltage, respectively.

The part of the current which is in phase with the voltage is called the active current component, while the current component orthogonal to the voltage is the reactive component.

$$P = U \times I_{re} \tag{2.3}$$
$$Q = U \times I_{im} \tag{2.4}$$

where

I_{re}	Is the real current component (active component)
I_{im}	Is the imaginary current component (reactive component)

2.6.2 Reducing voltage drops with reactive power

Equations (2.5) - (2.7) describes the voltage drop over an impedance drawn in Figure 2.5, expressed with the current split in its respective real and imaginary components. It can be seen from the very last part of Equation (2.7) that the reactive current component I_{im} compensates part of the voltage drop, due to the positive sign. By increasing I_{im} further, the resulting voltage U_2 will drop less. This

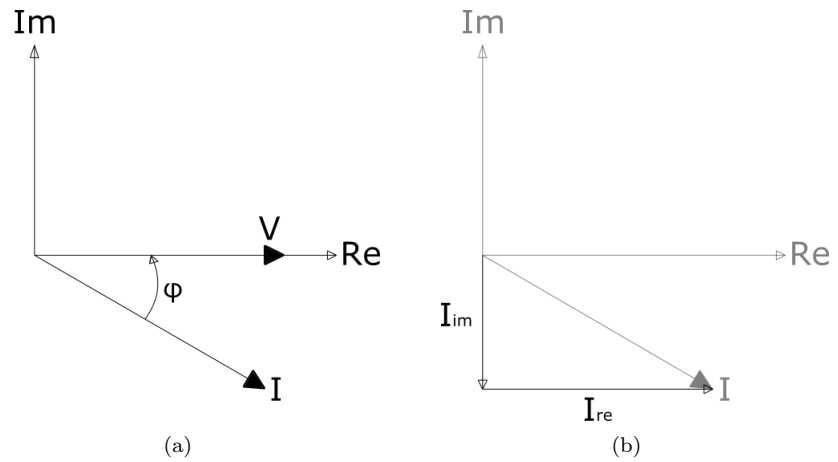

Figure 2.4: The current, composed of an active and reactive component, lags behind the voltage V with the angle ϕ

also causes U_2 to lag farther behind U_1 than what it otherwise would, as shown in Figure 2.6(b).

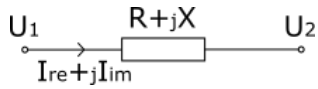

Figure 2.5: The discrepancy between U_2 and U_1 is the voltage drop over the impedance ($R+_jX$)

$$U_2 = U_1 - U_{drop} \tag{2.5}$$
$$U_2 = U_1 - (R + jX)(I_{re} + jI_{im}) \tag{2.6}$$
$$U_2 = U_1 - j(I_{im}R + I_{re}X) - I_{re}R + I_{im}X \tag{2.7}$$

where

U_1	Is the voltage at the beginning of the line
U_2	Is the voltage at the end of the line
U_{drop}	Is the voltage drop over the impedance
R	Is the resistance
X	Is the reactance

With a lagging power factor of 0.98, giving us an angle of 11.5°, Q amounts to 20 % of S. If the angle is leading, the absolute value of Q remains the same while the sign will be negative instead of positive. Reactive power is now injected to the system by the load, instead of delivered to the load from the system. A leading power factor 0.7 ($\phi \approx$ - 45°) gives us a Q that is 50 % of S.

Q was not measured by the smart meters in Steinkjer, but the local DSO assumes the PF in its grid to equal 0.98 lagging.

Since an increase in Q (and with this $I_i m$) can reduce the voltage drop, the technique that is reactive power control is proposed as a way to help increase the grid voltage stability.

A suggested technique to help integrate EVs and other high-power loads, is to inject reactive power at the location of the load in question, to reduce the voltage drop [5]. This will increase the apparent power flow in the connecting lines unless the active power consumption is reduced accordingly.

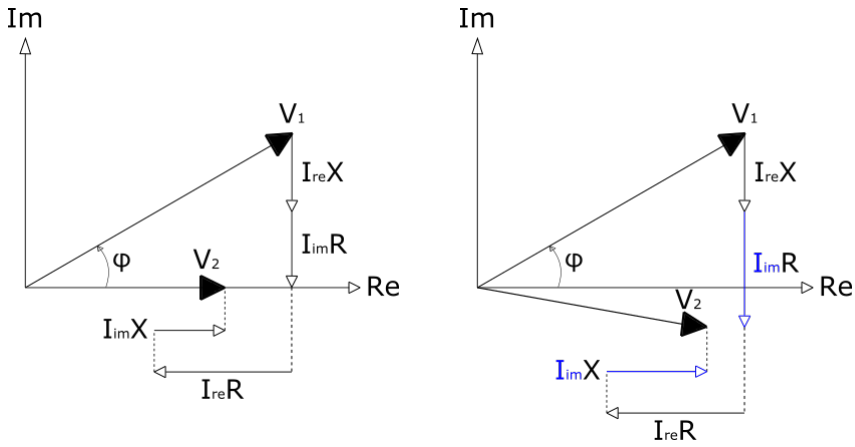

Figure 2.6: A visualization of the vector summation from U_1 to U_2. The dashed lines below the real axis are used to separate the horizontal vector sums in order to make the diagrams more easy-to-read.

2.7 Load flow studies

When solving a load flow problem (also called a power flow problem), the voltage magnitude and phase angle is computed at every node in a given network, assuming balanced three-phase conditions. Each bus k in the system has assigned four variables: Voltage magnitude V_k, phase angle δ_k, net active power P_k and net reactive power Q_k. The bus type is either a *slack/swing bus*, a *load bus* or a *generator bus*. The swing bus is the reference for the rest of the system, with a voltage defined as 1 p.u. and zero phase angle.

The problem is constructed by making a bus admittance matrix Y_k, which sums up the admittances between all interconnected buses in a system. With the self-admittance of each bus along the diagonal and the admittance value between the different buses on the off-diagonal. Starting with this, the power flow equations (2.13) - (2.14) can be derived as shown on page 16 [14].

2.7.1 Regarding three-phase power flow

To solve the load flow problems, MATPOWER must assume the grid in question to be balanced between its phases at all times, and the same assumption will therefore have to be made for the model in this thesis. The loads in the actual distribution grid will not necessarily be connected to their respective phases in a uniform manner, as they are for the most part not connected as three-phase loads, but rather connected across two phases in the case of an IT-grid. Excessive loading on a single phase may cause dissymmetry between the respective phases and worsen the results.

$$\mathbf{I} = \mathbf{Y_{bus}}\mathbf{V} \tag{2.8}$$

where for each bus, I_k and S_k is

$$I_k = \sum_{n=1}^{N} Y_{kn}V_n \tag{2.9}$$

$$S_k = P_k + jQ_k = V_k I_k^* \tag{2.10}$$

Combining these gives

$$P_k + jQ_k = V_k \left[\sum_{n=1}^{N} Y_{kn}V_n\right]^* \tag{2.11}$$

which with the notation
$\mathrm{V}_n = |\mathrm{V}_n|\mathrm{e}^{\delta_n}$ and Y_{kn}=$|\mathrm{Y}_{kn}|\mathrm{e}^{\theta_{kn}}$ gives

$$P_k + jQ_k = |V_k| \sum_{n=1}^{N} |Y_{kn}||V_n| e^{\delta_k - \delta_n - \theta_{kn}} \tag{2.12}$$

Finally, using Euler's formula, Equation (2.12) can ble split into:

$$P_k = |V_k| \sum_{n=1}^{N} |Y_{kn}||V_n| cos(\delta_k - \delta_n - \theta_{kn}) \text{ and} \tag{2.13}$$

$$Q_k = |V_k| \sum_{n=1}^{N} |Y_{kn}||V_n| sin(\delta_k - \delta_n - \theta_{kn}) \tag{2.14}$$

.
where

$\mathbf{I}$	is a vector of currents injected into each bus in the system
$\mathbf{Y}$	is the bus admittance matrix
$\mathbf{V}$	is a vector of all bus voltages
δ_k, δ_n	is the voltage angle at bus k and n, respectively, with reference to the slack bus
θ_{kn}	equals $\delta_k - \delta_n$

Equation (2.13) and (2.14) can be solved with numerical methods like Newton-Raphson or Gauss-Seidel, which is what load flow software does.

2.7.2 MATPOWER

MATPOWER is an open source subset of packages available for use in the MATLAB software to perform load flow and optimal load flow analyses [15], and will be used for conducting all load flow analyses in this thesis. The *runpf* function from MATPOWER takes in a single MATLAB struct file as input data; the MATPOWER case struct, or *mpc* for short. One mpc struct contains the necessary information for all nodes in the network for a given point in time, like the bus type and its corresponding known information.

The contents of an mpc struct is shown in Figure 2.7. The output from *runpf* has the same structure as the mpc struct, with the exception of the *branch*-part, which has four extra columns describing the active and reactive power flow in both directions. The discrepancy in absolute value between the active power flows in each line gives us the active power losses. The voltage magnitudes at each bus is expressed in p.u. in the bus-part of the mpc.

By running a load flow solution for every sample point in the grid with known power consumption values, the voltages and power flows in the network can be calculated.

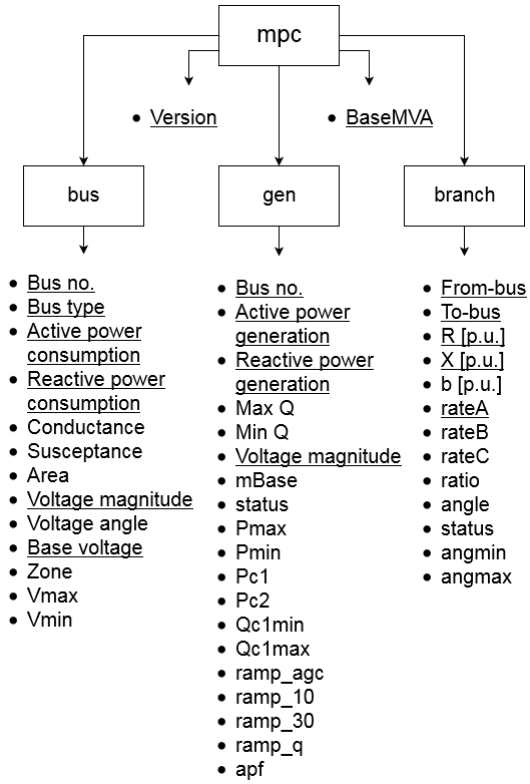

Figure 2.7: A flowchart depicting the structure of a matpower case struct

3 Data set

A summary of the original data set will be given together with a list of the information derived from it, and how it was done. The most important parts of the process will be described in detail in the following sections.

3.1 Description of the system

A single line diagram can be seen in Figure 3.1. It consists of the following main parts:

- A 500 kVA distribution transformer
- 20 distribution feeder lines, A1-M2, branching out from the transformer
- 54 end-user buses

In reality, there are 95 end-users present in the system, but some of these live in various forms of shared housing, like row houses or apartment blocks, thus sharing the same connection line. These larger nodes have been aggregated into single loads, and are marked with a larger, colorized symbol in the single line diagram. After this aggregation, the total number of end-users is 54.

The numbering of the end-users is the same as in the data delivered from the DSO, except that the numbering has been shifted to fill in any missing entries.

Three buses, no. 10, 32 and 53, are identified as an elderly care home, a grocery store and a school, respectively. 48 end-users are anonymized by the DSO, but display load profiles and a total energy consumption indicative to common households, and the remaining buses is marked as households.

3.1.1 Original data

The following data set was provided by the DSO:

- Hourly active power flow measurements for the year of 2012, for all end-users in the system
- A chart describing all interconnections in the system, and the types of cables being used.
- A separate smart meter measurement for a neighborhood in 2016, in which one household owns an EV

The active power measurements consists of 8784 measurements per end-user. This is due to 2012 being a leap year, thus consisting of 8784 hours.

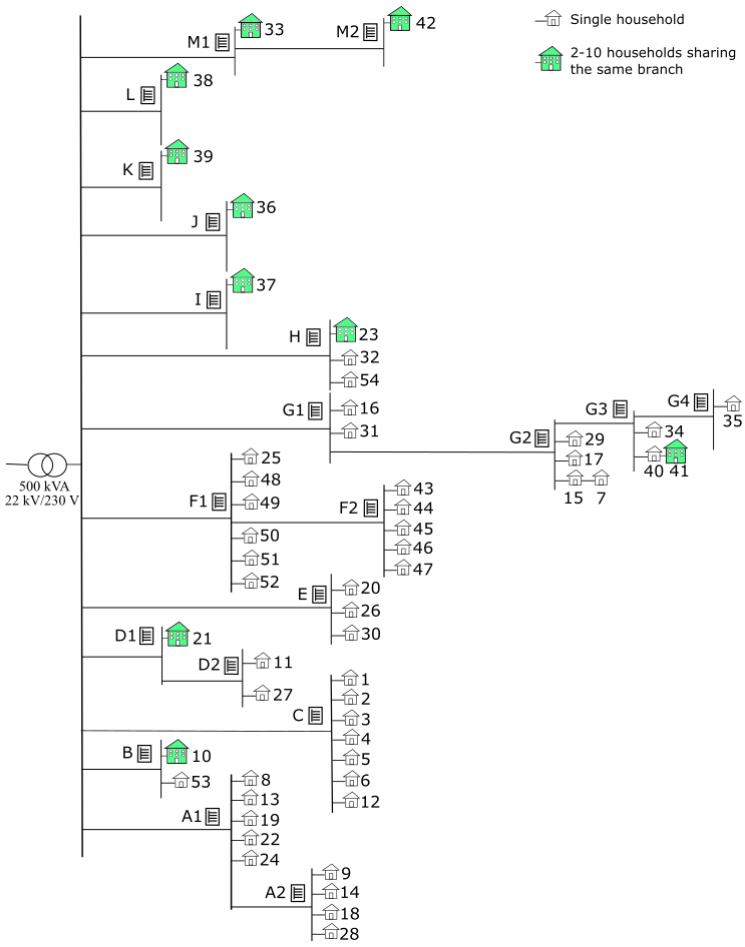

Figure 3.1: The grid in Steinkjer with its 54 consumer nodes, distributed over 20 feeder line connections

3.1.2 Derived data

The following information has been derived from this data:

- Hourly reactive power flow, based on the DSO's assumed power factor
- MVA ratings for all cables
- The single line diagram seen in Figure 3.1
- A empirical EV charging profile for a whole year

3.1.3 Cable MVA ratings

In Table 3.1, the 14 types of cables used in the system are listed.

In order to compare the grid power flows to the respective cable's rated power threshold, i.e. the *load ratio*, a maximum power rating had to be derived from the first column in the Table 3.1. The first four letters in the cable description designates the cable type in accordance with Nexans' code of practice [16], wherefrom the isolation type can be looked up.

The isolation type, cross-sectional area (third number, given in mm^2) and the conductor material is sufficient to look up the max ampere rating in for all cables in the corrigendum given by the Norwegian Electrotechnical Comittee [17]. Finally, the MVA rating was calculated with Equation (3.1).

$$MVA_{rating} = \frac{\sqrt{3} \times I_{cap} \times V_{\phi}}{1000000} \tag{3.1}$$

where

I_{cap}	Is the current-carrying capacity of the cable
V_{ϕ}	Is the phase voltage

Table 3.1: Cable types and their respective MVA rating

Cable code number	Isolation type	max A	MVA rating
PFSP 1X3X25 AL	PVC	69	0,0275
PFSP 1X3X50 AL	PVC	99	0,0394
PFSP 1X4X50 AL	PVC	99	0,0394
TFSP 1X3X150 AL	PEX	220	0,0876
TFSP 1X3X240 AL	PEX	290	0,1155
TFSP 1X3X95 AL	PEX	172	0,0685
TFXP 1X4X16 AL	PEX	64	0,0255
TFXP 1X4X50 AL	PEX	117	0,0466
TFXP 1X4X95 AL	PEX	172	0,0685
PFSP 1X3X10 CU	PVC	54	0,0215
PFSP 1X3X16 CU	PVC	70	0,0279
PFSP 1X3X2.5 CU	PVC	24	0,0096
PFSP 1X3X4 CU	PVC	33	0,0131
PFXP 1X4X16 CU	PVC	70	0,0279
Transformer			0,5000

3.1.4 Repairing data

As this specific smart meter data dump had not been inspected previously, it was discovered that some meters had malfunctioned at various times throughout the

year. 7 out of 74 consumers had less than 366 full days of data, and had to be sorted out manually. The missing periods of time were patched by comparing the existing data to neighboring consumption profiles, and copying in the remaining data from the most similar neighbor. The lengths of the missing data varied from days to a few months. An example of one of the patches i shown in Figure 3.2

The data gathering central is assumed to have blacked out or intentionally been disconnected for an hour at midnight, March 25th, as the consumption for all end-users were missing for that particular hour. The consumption for 23:00 was copied in for all of them as replacement. This is assumed to be negligible, as it only affected 0.011 % of the data set, in addition to the knowledge that consumption spikes rarely happen at that time of day.

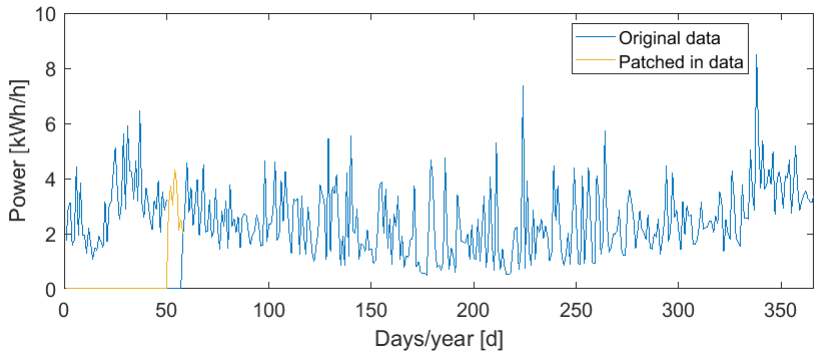

Figure 3.2: An example of a bus where the 41 hours in February had to be copied in from another household

3.2 Fitting all data to the MATPOWER format

To be able to run the model in MATPOWER, the given line impedances had to be converted to per unit values. This was done by setting V_{base} to 230 V and S_{base} to 10 MVA, and so Z_{base} could be found by calculating

$$Z_{base} = \frac{V_{base}^2}{S_{base}} \tag{3.2}$$

where

Z_{base}	Is the base impedance
V_{base}	Is the base voltage
S_{base}	Is the base apparent power

The resistance and reactance values were subsequently converted to per unit by dividing with Z_{base}.

The external power grid was modelled as an infinite bus connected to the main feeder, and acting as the generator in the system. The impedances and MVA rating of the transformer was modelled as a cable connected in series between the generator and the main feeder. This infinite bus acted as a slack bus with a constant voltage of 1 p.u. All end-users in the system were modelled as load buses. Finally, the bus bars between the transformer's feeder lines and the end-user branches were implemented in the model as load buses with zero active and reactive power consumption. This allows the user to add loads to them in a later stage of the study. The mentioned bus bars are denoted with letters A1-M2 in the single line diagram in Figure 3.1.

The MVA rating of the transformer was assigned to a virtual line which connects the transformer to the main feeder.

The smart meter readings were exported to MATLAB from Excel using the *xlsread* function. All of the parameters required for the mpc-struct except for the active and reactive power use, were exported to MATLAB as a template, wherein the active and reactive power consumption for each hour of the year was filled inn accordingly.

3.3 Deriving an EV charging pattern

A separate dataset containing smart meter measurements from a neighborhood in Nord-Trøndelag has been received from NTE for this purpose especially, in addition to the 2012-dataset on which the system model in this thesis is based on. One of the houses in this dataset is confirmed to own an EV.

To derive charging data from the EV-household, the household's base load must be subtracted from the total. A comparative base load has therefore been constructed by making an average load profile from the surrounding neighbors. By assuming that the EV adds an extra 3000 kWh to the household consumption, an average household consumption 3000 kWh smaller than the EV-household was created.

After subtracting the constructed average base load from the EV owning household, residual noise remained, resulting in rapid oscillations around the x-axis. To remove this, all values smaller than 2,7 kW were set to zero. This eliminated the noise left over from the subtraction without affecting the total area under the curve much, as approximately half of the values were below zero. Finally, all peaks larger than 7.3 kW were clipped down to 7.3 kW, as any remaining value higher than the maximum available charging power must be a residual value left over from the base household consumption. The resulting charging profile is shown in Figure 3.3, and an excerpt of this graph is shown in Figure 3.4, displaying eight days of energy consumption. A comprehensive visualization of the described working steps is available in appendix part B.

The area below the curve of the charging profile equals 3024 kWh. This is close to the expected yearly energy consumption for an EV, and it is therefore assumed that most of the consumption shown in the graph stems from EV charging.

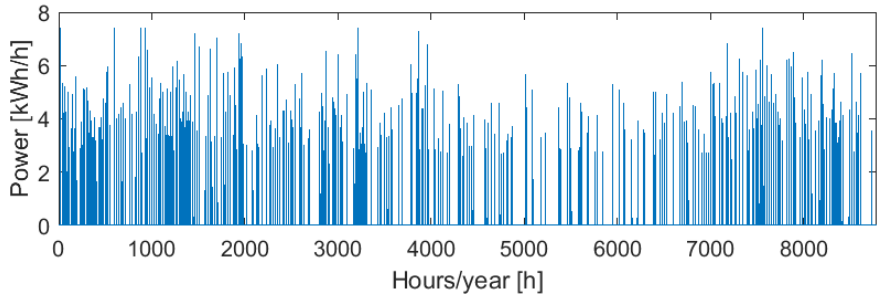

Figure 3.3: The proposed EV charging pattern

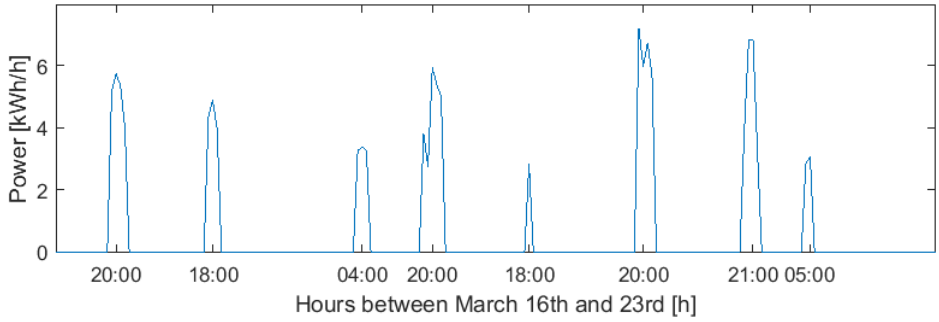

Figure 3.4: An excerpt of 8 consecutive days from the EV charging profile in Figure 3.3. The power spikes are marked with their respective time of day

4 Methodology and model description

The study will be conducted as 8784 individual load flow solutions - one for each hour of the year. To handle the data in an organized matter, as well as inserting and extracting data to and from the MATPOWER format, a series of MATLAB functions have been written to perform these operations in an ordered and efficient manner. The most important functions are listed in the appendix for the sake of ensuring transparency, and will be referred to with their respective appendix lettering in the following sections. The load flow results were found by running the *runpf* function for each hour of the year, with each respective mpc-struct as input per hour. The outputs were then stored in a nested output struct, which therefore contains 8784 structs in total.

4.1 Assumptions

- The maximal household charging rate is set to 7.3 kW, as this is the maximal charging rate in an IT-grid.
- It is assumed 0 EVs to be present in the grid when the data was collected in 2012. This is supported by the fact that the whole municipality had only 13 registered EVs dispersed over 38 075 inhabitants at that year [18] [19].

4.2 Assigning EV owners to the system

In this thesis, the degree of EV penetration is defined the following way:

$$\text{EV penetration} \equiv \frac{\text{End-users in the system}}{\text{EVs in the system}} \tag{4.1}$$

10 different EV penetrations from 10 % to 100 % with an incremental increase of 10 % between each case will be modeled. The peak voltage deviation and peak load ratio levels at all 20 feeder connections will be presented, along with a summary of any end-users experiencing a violation of the 10 % voltage deviation limit or an overloading with respect to the nominal power rating.

The EV charging profile is added on top of the existing household consumption at various buses in order to model different levels of EV penetration. 100 % EV penetration is in this thesis defined to correspond to 1 EV per household, which is rounded up for 95 end-users percentages given in Table 4.1. The buses which contain aggregations of multiple household consumption profiles are allowed to take in an equivalent number of EV loads.

Table 4.1: No. of EVs implemented in the different scenarios. Each increasing EV-share compounds on top of the previous one

% EV-share	**No. of EVs**	**Rounded up**
10	9,5	10
20	19	19
30	28,5	29
40	38	38
50	47,5	48
60	57	57
70	66,5	67
80	76	76
90	85,5	86
100	95	95

To construct the different EV penetration cases in a systematic order, the charging profiles have been added in accordance with a delegation array that keeps track of where the load profiles should be added in all cases. In the 10 % EV penetration case, the first 10 locations in the delegation array will be assigned their respective EV charging load. For 20 % EV penetration, the first 19 locations in the delegation array will be assigned their respective load, etc. This ensures a cumulative development from one EV penetration percent to another. The delegation array was made with the help of the *randperm* function in MATLAB. The random generator seed was reset to its default value in advance, to ensure reproducibility of the procedure.

It is desirable to avoid adding identical charging patterns to the different end-users, as that would not be a realistic scenario. The charging profile was therefore shifted forwards in time using the *circshift* function in MATLAB. To preserve the natural daily use pattern, the profile was only shifted a single hour back and forth in relation to its original pattern, before it was shifted 24 hours forward in time. The exact algorithm for adding the charging profile to the mpc struct is given in appendix part A.1.

4.3 Adding a fast charger to the system

To investigate the possible interaction between a fast charger and existing EV-loads, the system model developed for the 30 % EV penetration will be used as the base model. The fast charger will be modeled as a constant 22 kVA load. This provides a consistent worst-case scenario for the fast charger part of this thesis' data analysis.

The fast charger was added in three different ways:

1. Adding the fast charger load to the existing system without changing any other variables
2. Assuming the fast charger replaces the 5 EV loads closest to its location
3. Repeating 2), while also examining the effects of 15 different power factors at each location

Descriptions of how the model was prepared for these three cases are given in the following three sections.

4.3.1 Adding a fast charger - no other changes

Using equations (2.1)-(2.2) described in Chapter 2.6.1, P and Q are derived from the apparent power S and the angle ϕ. ϕ is derived from the power factor, which is assumed to be 0.98 lagging like the rest of the loads in the system.

The 22 kVA fast charger consumption was added to the existing consumption in the mpc struct, by adding the active and reactive components to it. The MATLAB script in appendix part A.3 was used for this purpose. A flowchart of the working steps for modifying the original mpc struct to the new case is shown in Figure 4.1.

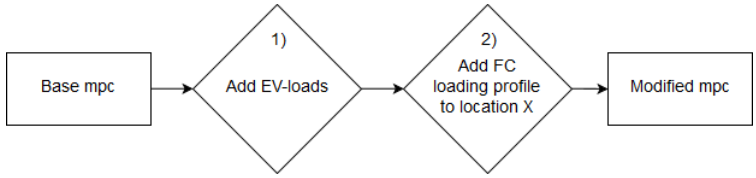

Figure 4.1: Flowchart: Adding a fast charger to the mpc struct

4.3.2 Assuming the charger replaces nearby EV charging

To investigate the effects of a common charging point like a fast charger on the existing EV loads, it will be assumed that the nearest 5 EVs charge at the common location instead of at their respective household. As only the interconnections between all nodes in the system and not their exact geographical location is given, the distances between the nodes in the single line diagram in Figure 3.1 will be used

as a substitution. The location for all EVs in the case with 30 % EV penetration is drawn in a copy of the single line diagram, given in appendix part D. The five EVs chosen to be replaced when placing the fast charger load at the 20 potential locations are given in appendix part C.1. A flowchart of the working steps for modifying the original mpc struct to the new case is shown in Figure 4.2.

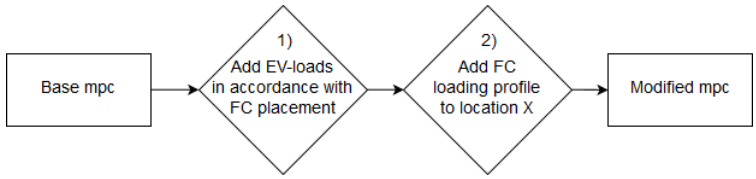

Figure 4.2: Flowchart: Adding a fast charger to the mpc struct and changing changing EV-loads

To build the appropriate mpc struct, the assigning of EVs had to be slightly modified 20 times in accordance with where the fast charger was going to be placed in each simulation. The function A.4 was used for this purpose, together with an array identical to Table C.1 containing information on which EVs would be affected by the placement. The fast charger could then be added as describes in chapter 4.3.1

4.3.3 Including reactive power control

While keeping the assumption that nearby EV-loads are substituted by the fast charger, each potential charger location will now in addition be tested for 15 different power factors in order to see the potential effects on the voltage level. It will be varied from 0.98 lagging to 0.74 leading, with an increment of 0.02 between each. A power factor of 0.74 corresponds to a -42.3° angle between the voltage and current phasor, and the resulting reactive power injection will be approximately equal to the active power consumption. A flowchart of the working steps for modifying the original mpc struct to the new case is shown in Figure 4.3.

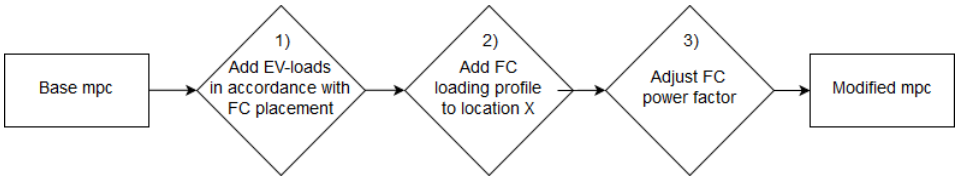

Figure 4.3: Flowchart: Including reactive power control to the fast charger

This was done by writing the function in appendix part A.5, which takes in the corresponding phase angle and adjusts P and Q accordingly, while keeping S constant at 22 kVA.

4.4 Finding an optimal fast charger location

Once all necessary data on how a base EV penetration and a fast charger placement at the potential locations will affect the voltage stability and power flows throughout the system, an attempt will be made to weigh these voltage deviation levels and total power loss in the system against each other. By doing this, a location for the fast charger which minimizes the overall voltage drops and system power losses can be chosen.

The average voltage deviation in the system can be weighed against the total power losses in the grid as a whole. The weighed-loss-voltage-factor (WLVF) is given in Equation (4.2), and returns a factor that is a weighed summation of the voltage deviations and the total power losses in the grid. By finding a WLVF-value for each of the 20 potential locations, the location with the smallest value for WLVF for the given weightages will be deemed the optimal location.

$$WLVF = w_1 \times V_{dev} + w_2 \times P_{loss}, \tag{4.2}$$

$$w_1 + w_2 = 1 \tag{4.3}$$

where

P_{loss_i}	Is the percent-wise increase in total system power losses when the FC is placed at location i, compared to the base case
V_{dev_i}	Is the average voltage deviation observed at all 20 feeder connections when an FC is placed at location i, in comparison to the base case
w_1	Weighing factor, determining the importance of voltage deviation
w_2	Weighing factor, determining the importance of the system power loss

4.5 Extracting results from MATPOWER

As the load flow results are stored in separate struct files in MATPOWER, which is sorted by hours, an iterative approach is used to collect the data. By looping through each struct file and collecting either load flow values or the voltage magnitude every iteration, load profiles and voltage profiles could be built for each respective bus. The processing was conducted in MATLAB, and a conceptual flowchart of the data collection is shown in Figure 4.4

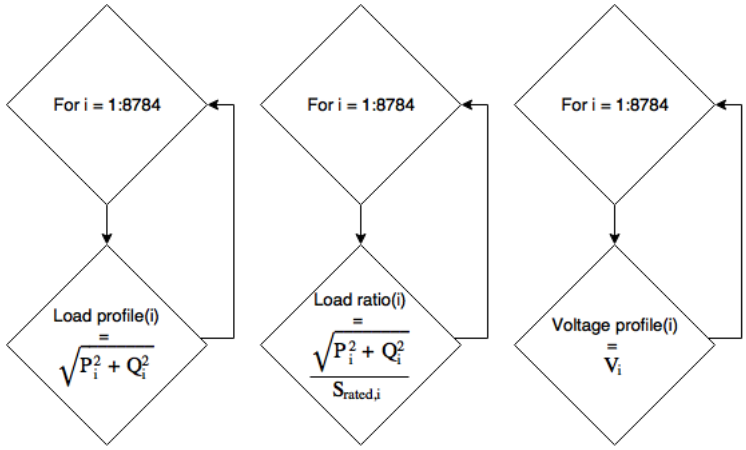

Figure 4.4: Flowcharts illstrating how the load flow and voltage magnitude data had to be acquired iteratively from MATPOWER. Each iterative loop represents the collection of a desired data point for a particular hour of the year

Since all extracted load and voltage profiles are referenced to a particular hour of the year between 1 and 8784, a script was written for the sole purpose of translating any hour to its respective date and time. E.g. the hour "1860" translates to "March 18 at 12:00". Although not a novel contribution, it has been made accessible in appendix part A.2 for future reference, as MATLAB does not have any in-built functions to easily perform this type of translation for leap years.

5 Results: Unmodified base case

The results in this part stems from the given raw data, before any virtual loads are added or any other changes are made.

5.1 Power capacities

The loading on the main transformer for the whole year is plotted in Figure 5.1, with a horizontal line denoting the rated capacity limit. A duration curve for the same data is shown in Figure 5.2.

The daily average loading on the transformer is plotted together with the daily average temperature in Figure 5.3. The temperature axis is reversed to emphasize the correlation between temperature and load demand in the network. The two load peak values in the first and second half of the year both reach 72 % loading capacity, and both occur during the two coldest days of the year.

In Figure 5.4, displays the average load ratio values for all end-users in the network, over the course of a week. That is, each of the 168 hours that constitutes the week, is an average of the load ratio value for all buses in the system at that particular hour, sampled over 52 weeks. Also shown is a summer and winter profile, which has been drawn from the main graph by defining the summer to last between weeks 21-37, and winter to be between weeks 46-11. The week numbers were chosen in accordance with a common definition of summer and winter, as the seasons containing days with a daily mean temperature above 10°C for summer days and below 0°C for winter days, which in this region typically are for the mentioned weeks [20]. The peak load consumption happens between 19:00 and 20:00 for all days of the week.

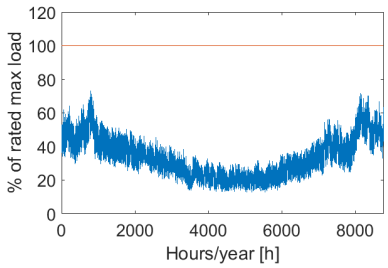

Figure 5.1: Transformer load for all hours

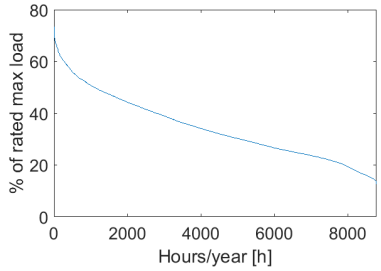

Figure 5.2: Sorted transformer loading

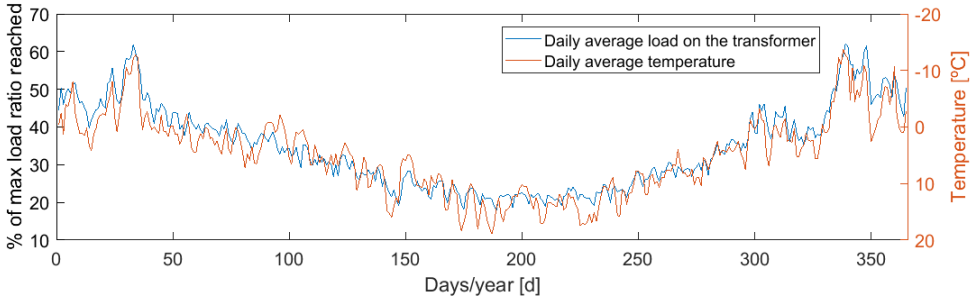

Figure 5.3: A comparison between the daily average temperature and daily average load on the transformer

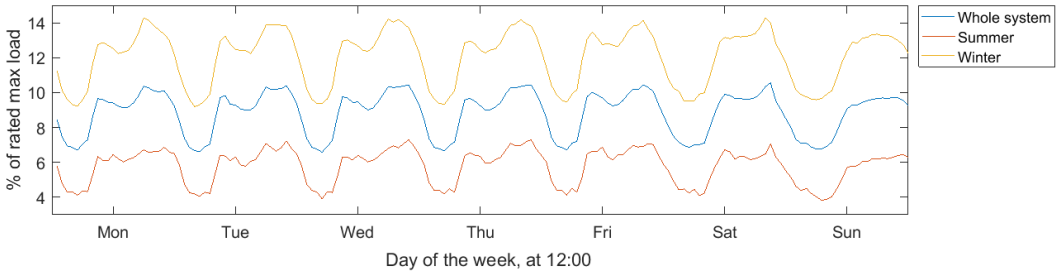

Figure 5.4: Average weekly load ratio for the whole system

Figure 5.5 shows the largest load ratio value reached during the year, for all end-users in the system. They are sorted after which feeder they are connected to.

With the exception of two cases, no end-users experienced overloading in relation to their cable MVA ratings. The exceptions are consumers 32 and 38, of which the former is almost consistently 20-40 % overloaded every day. This is a grocery store, and it is assumed that the provided cable information is wrong in this case, as the fuses did not blow once during the year. The latter, consumer 38, is a regular household. It reaches an overloading percentage of 1 % to 8 % for 6 hours throughout year. The rest of the end-users lie below their respective max loading capacity, and most stay below 60 % loading for all hours of the year.

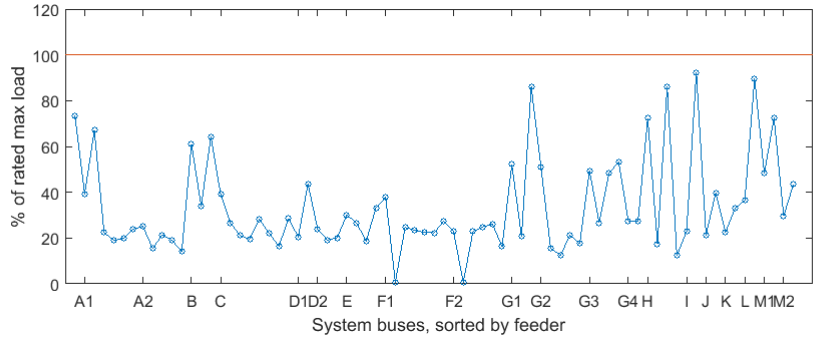

Figure 5.5: Largest load ratio value reached for all buses in the system, sorted by which feeder to which they are connected

5.2 Voltage levels

Figure 5.6 shows the largest load ratio value reached throughout the year, for all end-users in the system. They are sorted after which feeder they are connected to. It can be seen that the radial branch labeled "G1","G2","G3" and "G4" is the part of the network where the largest voltage deviations occur. However, no end-users were measured to experience a voltage deviation below 0.9 % p.u., and all but 4 locations stayed above 0.94 p.u. for the entire year. The four exceptions were all connected to either "G3" or "G4", and the voltage dip occurred during the two coldest days that year.

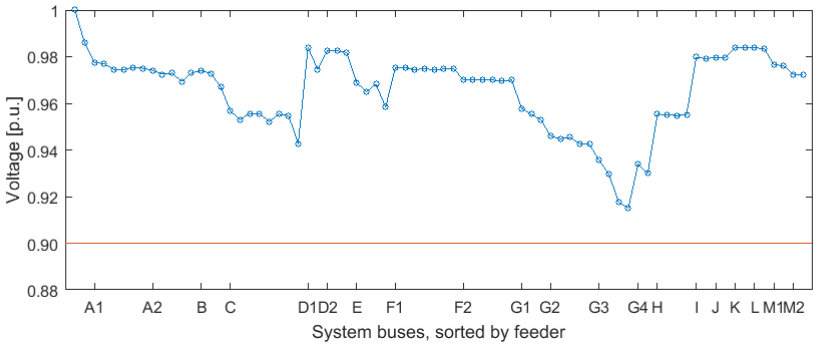

Figure 5.6: Lowest voltage magnitude reached for all buses in the system, sorted by which feeder to which they are connected

In Figure 5.7, a weekly average of the voltage level at all end-users in the system is given. It was constructed the same way as Figure 5.5, but by sampling voltage magnitudes instead of.

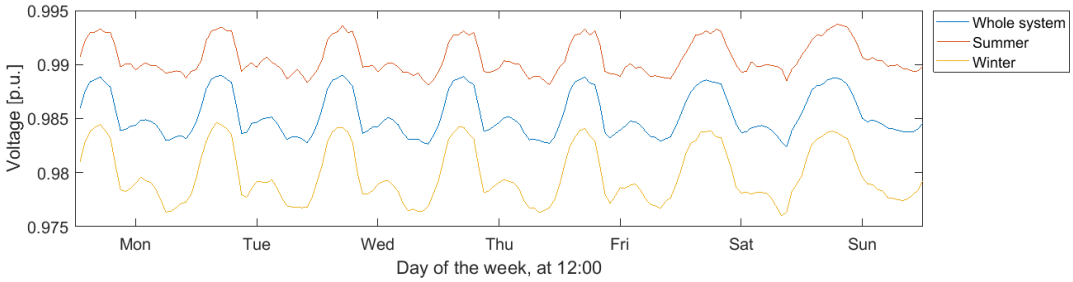

Figure 5.7: Average weekly voltage level for the whole system

When looking at the voltage level at the end of the distribution lines feeding the end consumers - denoted no. 55-74 in the network diagram - 18 out of 20 lines all deviate farthest from the ideal voltage level of 1 p.u. on either February 3rd, December 3rd or late at New Year's Eve. As with the line loading results, the two coldest hours in Steinkjer that year, at -12,7 and -13,7 degrees Celsius, happened during the two former dates.

6 Results - Implementing various EV penetrations

Load flow solutions have been run for 10 different EV penetration levels from 10 % to 100 % with an incremental increase of 10 % between each case, for all hours of the year. The following sections provide the most important results.

6.1 Power capacities

Figures 6.1 and 6.2 display the loading on the transformer during the case of 100 % EV penetration. The former figure is chronologically sorted, while the latter is sorted in a duration curve. They show that although the main transformer is significantly loaded during the winter season, it is only overloaded for a total of 12 hours.

Figure 6.3 displays how close each feeder line is to its maximum power transfer capacity, with the horizontal line showing the max capacity. None of the feeder lines were overloaded during any of the EV penetration cases.

In Figure 6.4, the load ratio for all buses in the network is shown. The end-users are sorted by which feeder they are connected to, as depicted in the single line diagram in Figure 3.1. They are sorted with the topmost end-user being listed first after each feeder, i.e. bus no. 1 is listed directly after the feeder labeled "C", and bus no. 12 is listed right before the feeder labeled "D1". In this figure, it can be seen that the aggregated end-consumer load connected to the radial labeled "I" reaches the nominal power capacity at a low level of EV penetration.

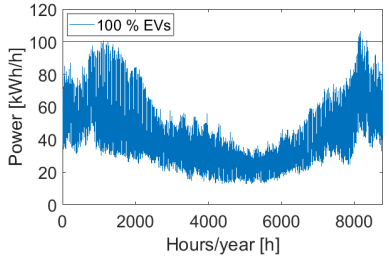

Figure 6.1: Transformer load for all hours, 100 % EV penetration

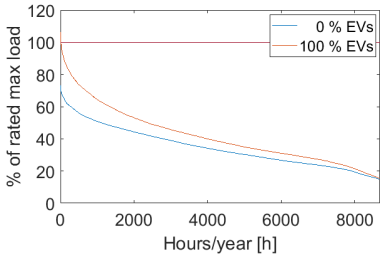

Figure 6.2: Sorted transformer loading. 11 hours lie above the rated max load

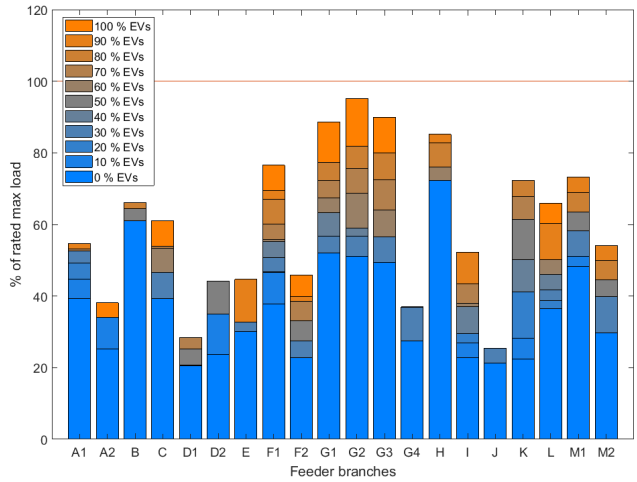

Figure 6.3: Largest load ratios for the feeder cables, for all EV penetrations

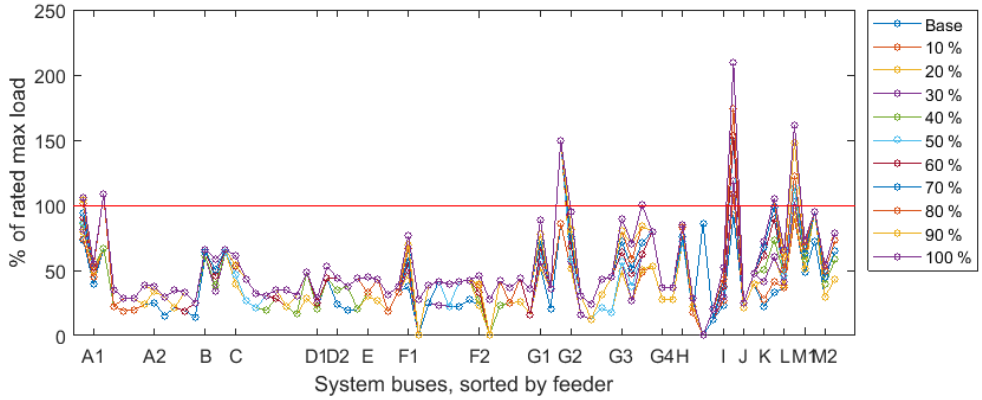

Figure 6.4: Largest load ratio value reached for all buses in the system, for all 10 EV penetration cases, sorted by which feeder to which they are connected

6.2 Voltage levels

The lowest voltage levels throughout the year at the end of each feeder line is displayed in Figure 6.5. Only the feeders labeled "G3" and "G4" reach a voltage level below 0.9 per unit, which occurs at the 100 % EV penetration level. The lowest voltage levels for all end-users in the grid is displayed in Figure 6.6. It can be seen that up to 6 end-users in addition to the feeder points themselves violate the lower voltage limit at one point, the first of which at the 60 % EV penetration level.

Figure 6.5 displays the largest voltage drops below 1 p.u. for each feeder line. The orange line shows the conventional maximum tolerable voltage deviation, which is 0,1 p.u. below 1,0 p.u. Feeder G3 and G4 drops below a voltage level of 0.9 p.u. at one point during the year. Figure 6.6 displays the largest voltage drops below 1 p.u. for all buses, sorted by the feeders to which they are connected.

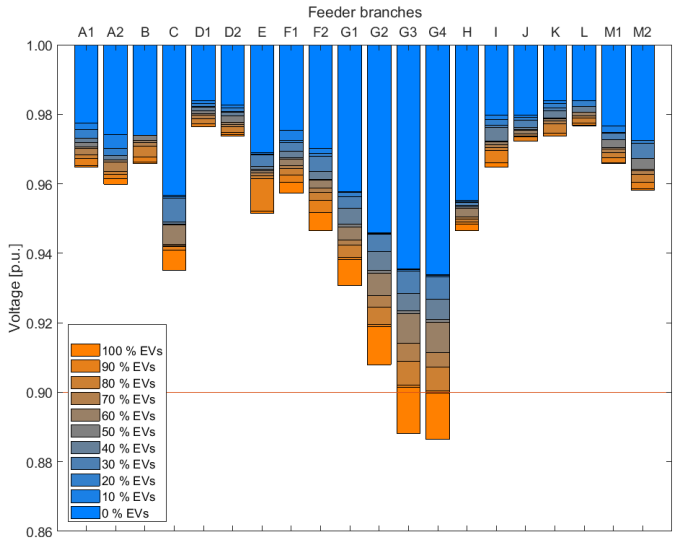

Figure 6.5: Largest voltage deviations below 1 p.u. for the feeder cables, for all EV penetrations.

Due to the described figures only illustrating the extreme values for the year, Table 6.1 provides supplementary information about the duration of the voltage limit or load limits being violated for the different EV penetrations. The duration is given in total hours throughout the year, and as a percentage of the total year.

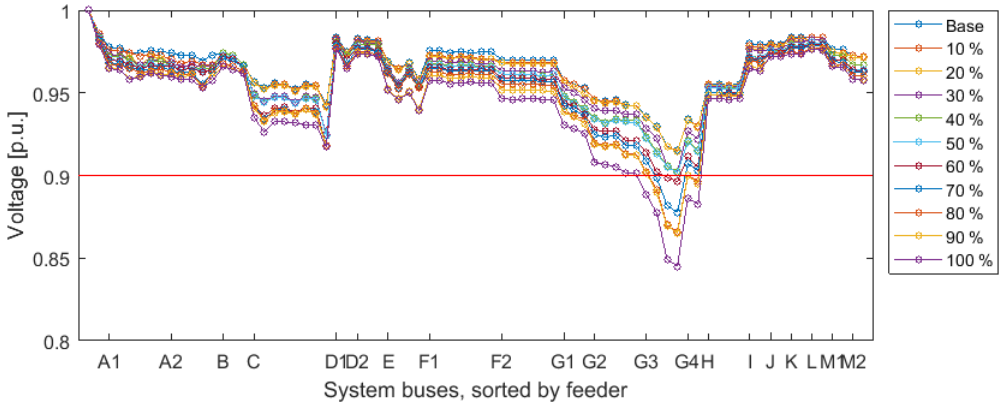

Figure 6.6: Lowest voltage magnitudes reached for all buses in the system, for all 10 EV penetration cases, sorted by which feeder to which they are connected

Table 6.1: A summary of the end-consumer state under all EV penetrations, stating the number of hours where one or more end-users experienced voltage or load ratio levels beyond their nominal limit for the whole year.

EV penetration	Overloaded hours		Undervoltaged hours	
0 %	0 h	0 %	0 h	0 %
10 %	5 h	0.06 %	0 h	0 %
20 %	134 h	1.53 %	0 h	0 %
30 %	135 h	1.54 %	0 h	0 %
40 %	212 h	2.41 %	0 h	0 %
50 %	215 h	2.45 %	0 h	0 %
60 %	285 h	3.24 %	2 h	0.02 %
70 %	361 h	4.11 %	11 h	0.13 %
80 %	363 h	4.13 %	31 h	0.35 %
90 %	478 h	5.44 %	37 h	0.42 %
100 %	511 h	5.81 %	75 h	0.85 %

7 Results - Fast charger implementation

The following sections provides results to help assess the effect of implementing a 22 kVA fast charger in the grid, and to investigate the potential benefits from reactive power control. Three variations of the fast charger implementation is shown. In all three of them, the fast charger is in turn added to all of the 20 potential locations, and the voltage levels and power losses will be calculated. Using these values, the weighed-loss-voltage-factor from Equation (4.2) is calculated, and the location returning the lowest value is considered to be the optimal location.

7.1 Fast charger base case

In Figure 7.1, the results for this case is labeled "Fast charger, base case". 10 optimal locations are given, one for each variation of the weightage. When w1 = 1.0, the focus is only on minimizing the average voltage deviation in the system. When w2 = 1.0, the total power losses in the system in minimized. In this case, location "L" was the optimal location regarding both voltage deviations and power losses. Hence, all intervening weightages also returned the same location.

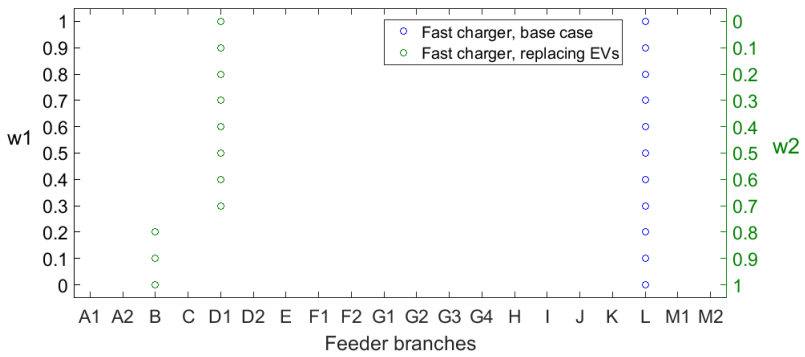

Figure 7.1:
In the base case, the optimal charger placement was at location L for all variations of w1 and w2. When assuming the FC replaces nearby EVs, the optimal charger placement changed to location D1 for all but the three highest values of w2, at which B took over

7.2 Fast charger substituting EV loads

The procedure was repeated for the new model by removing 5 nearest EV-loads. The new optimal locations for the different weightages is labeled as "Fast charger, replacing EVs" in Figure 7.1. It can be seen that the optimal charger placement is either location "B" or "D1". A placement at "D1" causes the least amount of overall voltage deviations in the grid, while placement at "B" results in the least amount of total power losses in the grid. The reason for this can be seen in Figure 7.2. By placing the fast charger at "B" and hence replacing the 5 nearest EVs, the feeder cables labeled "C" and "A1" were both alleviated. This caused the voltage to drop less than in the reference case.

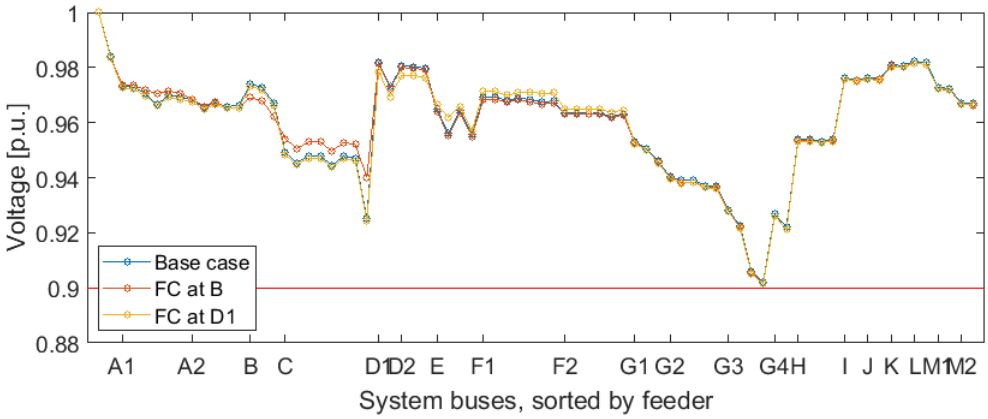

Figure 7.2: Resulting voltage deviations from placing a fast charger at location "B" and "D1", with the reference case plotted for comparison

7.3 Reactive power control

When investigating 15 different power factors at the location of the fast charger, 15 different plots of the same type as Figure 7.2 are produced; one for each power factor. The data sets will have to be three-dimensional to incorporate the extra set of variables, and an example of this is shown in Figure 7.3. The 20 feeder cables are shown along the x-axis, and the maximal voltage deviation throughout the year is shown along the z-axis. Along the y-axis are 15 different power factors along, thus making the plot three-dimensional. The fast charger has been placed at location "G4", which resulted in the largest amount of voltage deviation in the system. It can be seen that for a power factor of 0.74 leading, a large part of the voltage deviation has been negated by the reactive power injection.

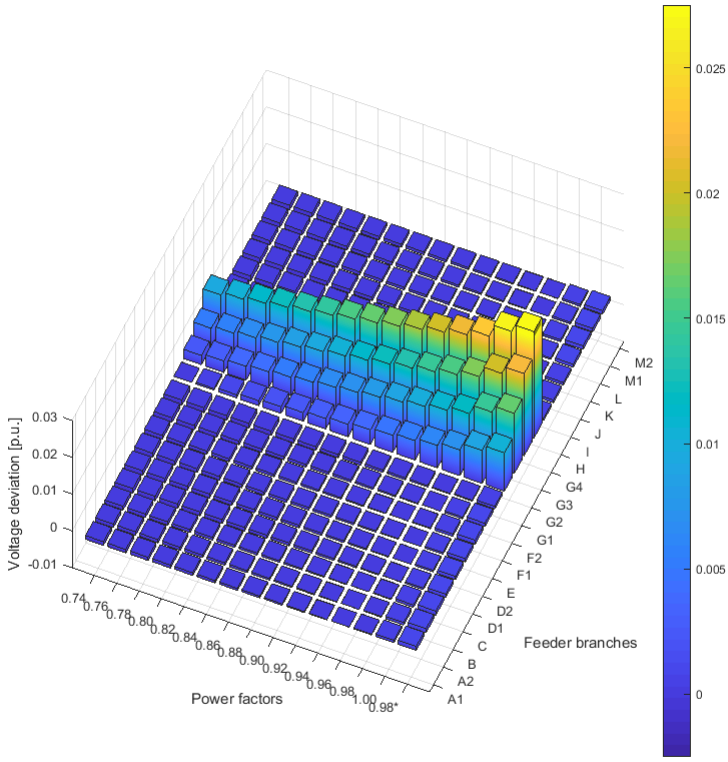

Figure 7.3: This plot shows the additional voltage deviation in all feeder locations when an FC is located at "G4", as compared to the base case

A more detailed plot for the system as a whole is shown in Figure 7.4, which plots the voltage deviation levels in the system for the standard power factor, and the lowest power factor.

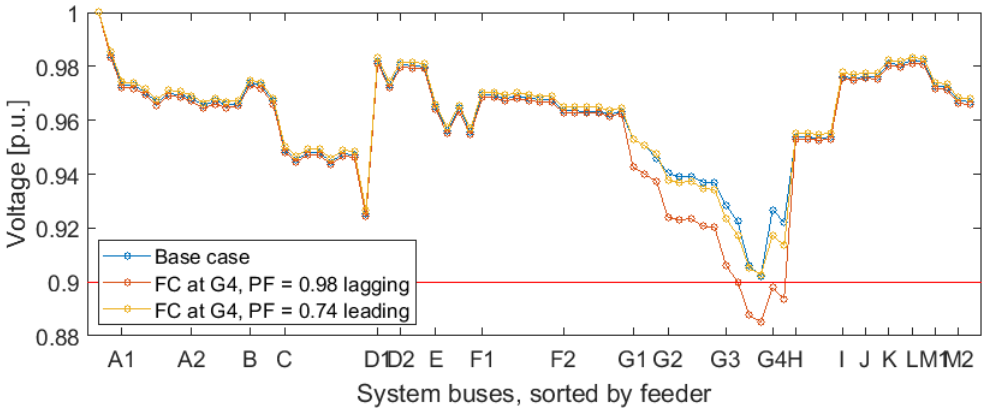

Figure 7.4: Locating the fast charger at G4 gave the most voltage deviations in the network

Table 7.1 summarizes the resulting optimal FC location for all power factors, and for all weightages w1 and w2. Even though reactive power compensation was shown in Figure 7.3 to give significant results, the relation between the locations for the same power factor remain mostly unchanged, thus resulting in either B or D1 remaining as the optimal location for all weightages.

Table 7.1: The optimal fast charger placement was at location B or D1 for all examined variations of w1, w2 and power factors

Power factor \ w1	0.0	0.1	0.2	0.3	0.4	0.5	0.6	0.7	0.8	0.9	1.0
0.98*	B	B	B	D1	D1	D1	D1	D1	D1	D1	D1
1.00	B	B	B	D1	D1	D1	D1	D1	D1	D1	D1
0.98	B	B	B	D1	D1	D1	D1	D1	D1	D1	D1
0.96	B	B	B	D1	D1	D1	D1	D1	D1	D1	D1
0.94	B	B	B	D1	D1	D1	D1	D1	D1	D1	D1
0.92	B	B	B	D1	D1	D1	D1	D1	D1	D1	D1
0.90	B	B	B	D1	D1	D1	D1	D1	D1	D1	D1
0.88	B	B	B	D1	D1	D1	D1	D1	D1	D1	D1
0.86	B	B	B	D1	D1	D1	D1	D1	D1	D1	D1
0.84	B	B	B	D1	D1	D1	D1	D1	D1	D1	D1
0.82	B	B	B	D1	D1	D1	D1	D1	D1	D1	D1
0.80	B	B	B	D1	D1	D1	D1	D1	D1	D1	D1
0.78	B	B	B	B	D1	D1	D1	D1	D1	D1	D1
0.76	B	B	B	B	D1	D1	D1	D1	D1	D1	D1
0.74	B	B	B	B	D1	D1	D1	D1	D1	D1	D1
w2	1.0	0.9	0.8	0.7	0.6	0.5	0.4	0.3	0.2	0.1	0.0

8 Discussion

The following sections discuss the findings from the results chapters.

8.1 Unmodified base case

Neither the transformer nor the other components in the network experienced overloading or violations of the minimum voltage level. However, several end-users experienced loading and/or voltage levels at near their nominal limit at some point during the year, as seen in figures 5.5 and 5.6.

8.2 Assessing the EV hosting capacity

A previous assessment of the EV hosting capacity of the distribution grids in the area had concluded with that a 25 % EV penetration with high charging currents (32 A) would violate the voltage limit in certain parts of the grid [12]. This is significantly less than the results in this thesis, where an EV penetration of 60 % was possible before the first voltage deviation incidents occurred.

None of the feeder cables became overloaded during the 100 % EV penetration case, as seen in Figure 6.5 and Figure 6.3) - only the end user cables branching out from the feeder cables did. If the same EV charging loads had been wired directly to feeders, the system as a whole could have managed the extra loading. Although the transformer experienced 12 hours of loading above its nominal power capacity, the hours occurred during the coldest day of the year. The cold temperature cools the transformer, and NVE assumes distribution transformers to tolerate up to 120 % loading during these conditions [3]. These details indicate a network that handles the EV charging loads better than the earlier thesis that assessed a nearby grid, stating that a 60 % EV penetration would load the main transformer with approximately 140 % of its nominal capacity [13].

8.3 Fast charger implementation

Figure 7.2 suggests that the replacement of other EV loads can lead to less voltage deviations in the network.

In [5], the use of reactive power control for charging EVs in general was concluded to be an effective measure to reduce the minimum voltage deviation in the system. Applying the same method for the fast charger in this thesis has shown similar results,

indicating in figures 7.3 and 7.4 that reactive power injection can be especially effective at the weaker parts of the grid.

8.4 Limitations of the study

All EV charging profiles used in this thesis stems from a single measurement. This measurement included the base load of the household, which had to be subtracted. One or more directly measured EV charging profiles over the course of a year would be superior to the one derived in this study, as no residual household consumption measurements would interfere the dataset, and no real charging data would have been lost as part of the subtraction process. Additionally, a larger sample would reduce the impact of any outliers in the individual data set.

When assessing the effect of having 5 EV loads being substituted by the fast charger load, the real distances between end-users was unknown. The judgement of which houses were the closest ones was therefore based on the literal distances between the houses in the network diagram. The cable lengths were drawn in the single line diagram to be indicative of their real length, but it is still an imprecise drawing. These results are therefore mainly applicable in a conceptual manner.

8.5 Sources of error

The smallest resolution of the model is 1 hour, as that was the sampling rate of the smart meters from which the power use data originated. It follows that any peak load value happening between two hourly samples would not be recorded.

The EV charging graph contains elements of uncertainty. A more ideal empirical EV charging graph would have been based on directly measured EV power consumption instead of having to extract it from the total household consumption, as the quality of the result will be sub-optimal. An example of this can be seen in the excerpt in Figure 3.4, where the two smaller power peaks at 04:00 and 05:00 most likely are residual noise from the household base consumption. The quality of the graph is also reduced by the minimum sampling resolution at 1 hour, as that makes it hard to sort noise from actual consumption when the day-to-day charging can be as short as less than two hours long. This is particularly relevant in this case, since the EV-owner charges with a 32 A circuit.

When delegating the EV-loads to the system, the factor at which EV-loads drew power at the same hour was significantly altered by the choice of shifting the load profiles back and forth with the *circshift* function in MATLAB. If this had not been done, all 95 EV loads in the system would have been identical and reached their semi-daily charging peak of 7.3 kW every single time. That would not be a realistic situation, nor is it normal to model. In a report where NVE explored different EV-behavior scenarios, a maximum charging simultaneity factor of 70 % was used

as a worst-case scenario. In this thesis, the simultaneity factor for charging was 33 %, due to the shifting of the charging profile. The 2017 survey by the Norwegian EV Association reported a max simultaneity factor of 22 %, which occurred at 04:00 at night after a continuous build-up from 19:00. The survey is, however, based on a guesswork from the respondents and not actual measurements.

9 Conclusion

The conclusion of this thesis will answer the research questions stated in chapter 1.2, in the same order as they were originally listed:

- The current state of the grid is good, as no end-users or branches violate the minimum voltage level of 0.9 p.u., nor is any nominal power transfer limits violated at any hour for the whole year.
- The EV hosting capacity is good for a majority of the end-users. For the case with 100 % EV penetration, all but 6 end-users stay above the minimum voltage limit at all hours of the year, and all but 6 end-users stay below the nominal cable power rating at all hours of the year. The main transformer is overloaded for a few hours, but only during the time of year where it is expected to tolerate the load due to the cold outside temperature. When restricting EV penetration to comply with the limitations of all end-users in the system, the distribution grid can tolerate a 50 % EV penetration with regards to voltage, and between 10 % to 20 % EV penetration with regards to the rated power of the weakest cable.
- Implementing a fast charger in the grid with a standard power factor of 0.98 lagging caused significant voltage deviations at several locations, the worst of which reached an extra voltage deviation close to 0.03 p.u. By assuming that the nearest 5 EV charging loads were replaced by the fast charger, the largest voltage deviations in the network were significantly reduced.
- Injecting reactive power at the location of the fast charger gave significant results. By injecting reactive power corresponding to a power factor of 0.74 leading, the fast charger was successfully implemented in the weakest part of the grid without violating the minimum voltage level requirement of 0.9 p.u.

By utilizing the voltage stabilizing properties of injecting reactive power, larger loads like a fast charger or a large EV household charger can be installed in weaker parts of a power grid than would otherwise be possible.

10 Further work

This thesis is written while the rollout of smart meters in Norway is happening. The new meters will hopefully increase the amount of accessible data on EV-charging in the coming years, making it possible to fine-tune models like the one used in this thesis. It would be especially interesting to attain and analyze directly measured yearly consumption profiles from EVs all over the country, as use patterns and daily energy consumption might differ between regions.

It would be interesting to look at the technical feasibility and expected-cost-of-use case where all 95 end-users with their respective EVs shared a smaller number of common charging connection points, instead of each household having their own charging station. For row houses and other households living in close proximity to each other, one could imagine a scenario where everyone charges "at home", but the chargers themselves are interconnected instead of being wired through their respective household circuit. Several different measuring systems can be envisioned to allocate the energy costs to the right EV user without introducing too much extra complexity for the user, and the total power drawn from the grid could more easily be observed and controlled.

As the coldest days of the year in many cases can be predicted by the weather services, a practical pilot study could be conducted where the EV owners are incentivized to not charge their respective EVs that particular day. A message could be sent a day beforehand, informing the EV-owning end-users of a certain discount being given to their respective power bill if they choose not to charge their EV the next day. This would be more of a social analysis, as the necessary equipment is already in place. Various price incentives, responses and subsequent effects on the grid could then be gathered and compared.

A study analogous to this one, but applied to a meshed grid, may provide other interesting results.

Bibliography

[1] Linda Ager-Wick Ellingsen, Bhawna Singh, and Anders Hammer Strømman. *The size and range effect: lifecycle greenhouse gas emissions of electric vehicles.* 2016.

[2] IEA International Energy Agency. *Global EV outlook.* 2017. https://www.iea.org/publications/freepublications/publication/GlobalEVOutlook2017.pdf [Online - collected 16-10-2017].

[3] Christer S. Skotland, Eirik Eggum, and Dag Spilde. *Hva betyr elbiler for strømnettet?* NVE - Norwegian Water Resource and Energy Directorate, Oslo, Norway. 2016.

[4] NVE Norwegian Water Resource and Oslo Energy Directorate. *Ny kraft: Endelige tillatelser og utbygging - 3. kvartal.* 2017.

[5] Katarina Knezovic. *Phase-wise enhanced voltage support from electric vehicles in a Danish low-voltage distribution grid.* 2016.

[6] Elbilforeningen. *Norwegian EV market.* 2017. https://elbil.no/english/norwegian-ev-market/ [Online - collected 05-Dec-2017].

[7] Norwegian Public Roads Administration. *Kjøretøybestanden i Norge.* 2017. *www.vegvesen.no/_attachment/1899542/binary/1187366?fast_title=Kj%C3%B8ret%C3%B8ybestanden+i+Norge+2007+-+2016.pdf.pdf* [Online - collected 04-01-2017].

[8] Eilif Hugo Hansen. *Elektroinstallasjoner.* textbook, 2010. ed. trondheim, norway: Classica. 2010.

[9] Norwegian Directorate for Civil Protection. *Lading av elektriske biler - Charging electrical cars.* 2015. www.dsb.no/globalassets/dokumenter/elsikkerhet-els/veiledninger-pdf/elbil$_i$*nstallatoer.pdf*[*Online* – *Collected*02 – 01 – 2018].

[10] Norsk Elbilforening - The Norwegian Electric Vehicle Association. *Elbilisten 2017.* Questionnaire - sent from the author on request. 2017.

[11] Norsk Elbilforening - The Norwegian Electric Vehicle Assiciation. *Kontaktene man bruker med elbil.* 2016. https://elbil.no/kontaktene-man-bruker-med-elbil/ [Online - Collected 09-01-2018].

[12] Tonje Rian. *Nettmessige konsekvenser ved økt grad av elbillading i distribusjonsnettet.* NTNU, Master's thesis, Trondheim, Norway. 2017.

[13] Åshild Vatne. *Analysis of Large Scale Adoption of Electrical Vehicles and Wind Integration in Nord-Trøndelag.* NTNU, Master's thesis, Trondheim, Norway. 2012.

[14] J. Duncan Glover. *Power system analysis & design.* 6th ed., 2017.

[15] R. D. Zimmermann , C.E. Murillo-Sánchez , R. J. Thomas. *MATPOWER: Steady-State Operations, Planning and Analysis Tools for Power Systems Research and Education. Power Systems, IEEE Transactions on, vol. 26, no. 1, pp. 12-19*, 2011.

[16] Nexans. *Kabelboka: Håndbok for e-verkskabler - "The cable book: Manual for electricity works cables*, 2014.

[17] Norwegian Electrotechnical Committee. *Elektriske lavspenningsinstallasjoner - Electrical low valtage installations* (5. ed., vol. 400:2014.

[18] Kommuneprofilen. *Kommuneprofilen - personbiler etter type drivstoff.* 2017. www.kommuneprofilen.no/Profil/Samferdsel/DinRegion/samf_drivstoff_region-.aspx, [Online - collected 05-12-2017].

[19] Kommuneprofilen. *Kommuneprofilen - befolkningsstatistikk etter kommune.* 2017. www.kommuneprofilen.no/profil/Kommunefakta/Befolkning_kommune.aspx, [Online - collected 05-12-2017].

[20] Store Norske Leksikon v/Mamen, J. https://snl.no/%c3%a5rstider_-_klima [online - collected 02-01-2018]. 2009.

A MATLAB scripts

In this part of the appendix, the most important MATLAB-functions written for the data analysis part is given.

A.1 Adding EV charging profiles to the network model

addToMpc

```
function [mpc_plus_EV] = addToMpc(mpc_all, EV_charging_profile,
    EV_owner_array)
% ADDTOMPC(mpc,EV charging profile, EV owner array)
% Returns an mpc-struct where the EV charging profile has been
% quasi-stochastically added to all buses named in the EV owner
% array.

mpc_plus_EV = mpc_all;
for i = 1:31  % Creating an index for the circshift function.
    foo(i*3-1) = 24*i-1;
    foo(i*3)   = 24*i;
    foo(i*3+1) = 24*i+1;
end
foo = circshift(foo,-1);
foo(94) = 767;
foo(95) = 768;

phi = acosd(0.98);
for k = 1:length(EV_owner_array)
    EV_charging_profile_shifted     = circshift(EV_charging_profile,
    foo(k));
    for i = 1:8784
        mpc_plus_EV.mpc(i).bus(EV_owner_array(k),3) = mpc_plus_EV.mpc(
    i).bus(EV_owner_array(k),3) + EV_charging_profile_shifted(i);
        mpc_plus_EV.mpc(i).bus(EV_owner_array(k),4) = mpc_plus_EV.mpc(
    i).bus(EV_owner_array(k),4) + EV_charging_profile_shifted(i)*tand(
    phi);
    end
end
```

A.2 Translating a given hour to its respective date and time

```
function [output_string] = hourToDate(hour)
% HOURTODATE(hour)
% Only applicable for leap years.
day = round(hour/24);
if day < 31
    month = 'January';
    hours_left = hour;
elseif day <= (31+29)
    month = 'February';
    hours_left = hour-31*24;
elseif day <= (31+29+31)
    month = 'March';
    hours_left = hour-(31+29)*24;
elseif day <= (31+29+31+30)
    month = 'April';
    hours_left = hour-(31+29+31)*24;
elseif day <= (31+29+31+30+31)
    month = 'May';
    hours_left = hour-(31+29+31+30)*24;
elseif day <= (31+29+31+30+31+30)
    month = 'June';
    hours_left = hour-(31+29+31+30+31)*24;
elseif day <= (31+29+31+30+31+30+31)
    month = 'July';
    hours_left = hour-(31+29+31+30+31+30)*24;
elseif day <= (31+29+31+30+31+30+31+31)
    month = 'August';
    hours_left = hour-(31+29+31+30+31+30+31)*24;
elseif day <= (31+29+31+30+31+30+31+31+30)
    month = 'September';
    hours_left = hour-(31+29+31+30+31+30+31+30)*24;
elseif day <= (31+29+31+30+31+30+31+31+30+31)
    month = 'October';
    hours_left = hour-(31+29+31+30+31+30+31+30+31)*24;
elseif day <= (31+29+31+30+31+30+31+31+30+31+30)
    month = 'November';
    hours_left = hour-(31+29+31+30+31+30+31+31+30+31)*24;
elseif day <= (31+29+31+30+31+30+31+31+30+31+30+31)
    month = 'December';
    hours_left = hour-(31+29+31+30+31+30+31+31+30+31+30)*24;
end
date       = ceil(hours_left/24);
hours_left  = hours_left - date*24 + 24;
if hours_left < 10
    output_string = [month, ' ', num2str(date), ' at 0', num2str(
    hours_left) ':00'];
else
    output_string = [month, ' ', num2str(date), ' at ' , num2str(
    hours_left) ':00'];
end
end
```

A.3 Adding a fast charger profile to an existing mpc-struct

```
function [mpc_plus_FC] = addFastChargerToMpc(mpc_all,
    FC_charging_profile, FC_location)
% ADDFASTCHARGERTOMPC(mpc, FC_charging_profile, FC_location)
% Assumes PF = 0.98 and adds a constant 22 kVA load to the assigned
    location

mpc_plus_FC = mpc_all;
power_factor = 0.98;
phi = rad2deg(acos(power_factor));

S = 0.022;
P = S*power_factor;
Q = sqrt(S^2-P^2);

for i = 1:8784
    mpc_plus_FC.mpc(i).bus(54+FC_location,3) = P;
    mpc_plus_FC.mpc(i).bus(54+FC_location,4) = Q;
end
```

A.4 Making modified mpc-structs, with different placement of EV loads

```
function [mpc_plus_EV] = addToMpc_modified(mpc_all,
    EV_charging_profile, EV_owner_array,exception_array)
% ADDTOMPC(mpc,EV charging profile, EV owner array)
% Returns an mpc-struct where the EV charging profile has been
% quasi-stochastically added on top of all buses named in the EV owner
% array. This version skips the households listed in exception_array,
    while assigning the remaining EV loads in the same way as in the
    original case.
mpc_plus_EV = mpc_all;
phi = acosd(0.98);

for i = 1:31 % Creating an index for the circshift function.
    foo(i*3-1) = 24*i-1;
    foo(i*3)   = 24*i;
    foo(i*3+1) = 24*i+1;
end
foo = circshift(foo,-1);
foo(94) = 767;
foo(95) = 768;

for k = 1:length(EV_owner_array)
    EV_charging_profile_shifted     = circshift(EV_charging_profile,
    foo(k));
    X = EV_owner_array(k);
    if((X~=exception_array(1))&&(X~=exception_array(2))&&(X~=
    exception_array(3))&&(X~=exception_array(4))&&(X~=exception_array
    (5)))
```

```
        for i = 1:8784
            mpc_plus_EV.mpc(i).bus(X,3) = mpc_plus_EV.mpc(i).bus(X,3)
    + EV_charging_profile_shifted(i);
            mpc_plus_EV.mpc(i).bus(X,4) = mpc_plus_EV.mpc(i).bus(X,4)
    + EV_charging_profile_shifted(i)*tand(phi);
        end
    elseif X==exception_array(1) % Ensuring that only 5 EVs are
    removed.
        exception_array(1)=0;
    elseif X==exception_array(2)
        exception_array(2)=0;
    elseif X==exception_array(3)
        exception_array(3)=0;
    elseif X==exception_array(4)
        exception_array(4)=0;
    elseif X==exception_array(5)
        exception_array(5)=0;
    end
end
```

A.5 Changing the power factor at a given bus in mpc

```
function [mpc_changed] = changePowerFactorInMpc(mpc, feeder_number,
    phi)
% CHANGEPOWERFACTORINMPC(mpc, feeder_number, power_factor)
% Adjusts the Q injection at the specified bus.

mpc_changed = mpc;
S = 0.022;
P = S*cosd(phi);
Q = S*sind(phi);

for i = 1:8784
    mpc_changed.mpc(i).bus(54+feeder_number,3) =  P;
    mpc_changed.mpc(i).bus(54+feeder_number,4) =  Q;
end
```

B EV charging profile derivation

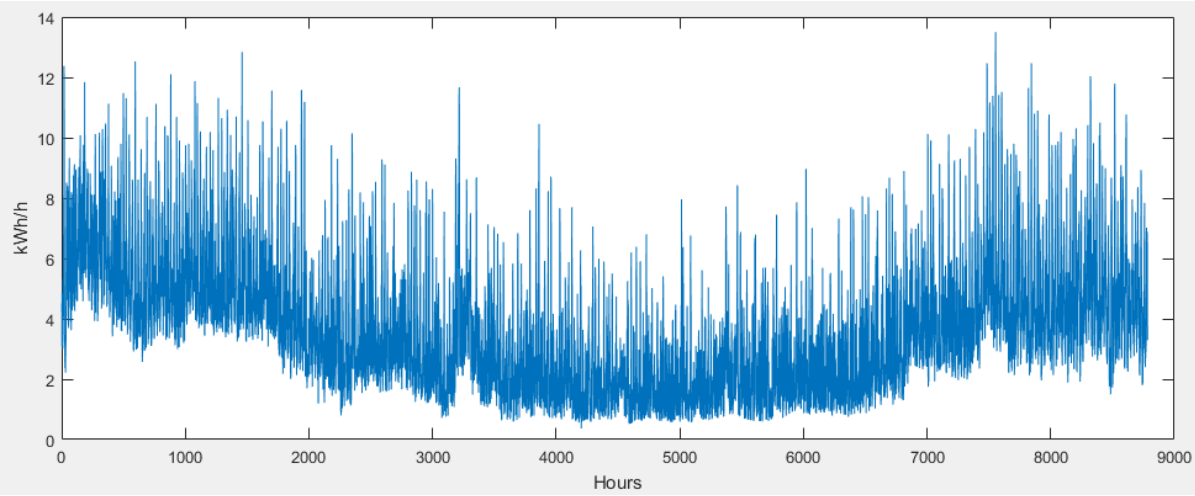

This is the basis of the charging graph: A smart meter measurement of a household confirmed to be own an EV. The data is from from 2016, and the house is in Steinkjer.

The goal is to attempt to withdraw the house base load, leaving us with only the EV charging load. The result is expected to be far from perfect, but the resulting graph has been deemed to fit its purposes in this thesis.

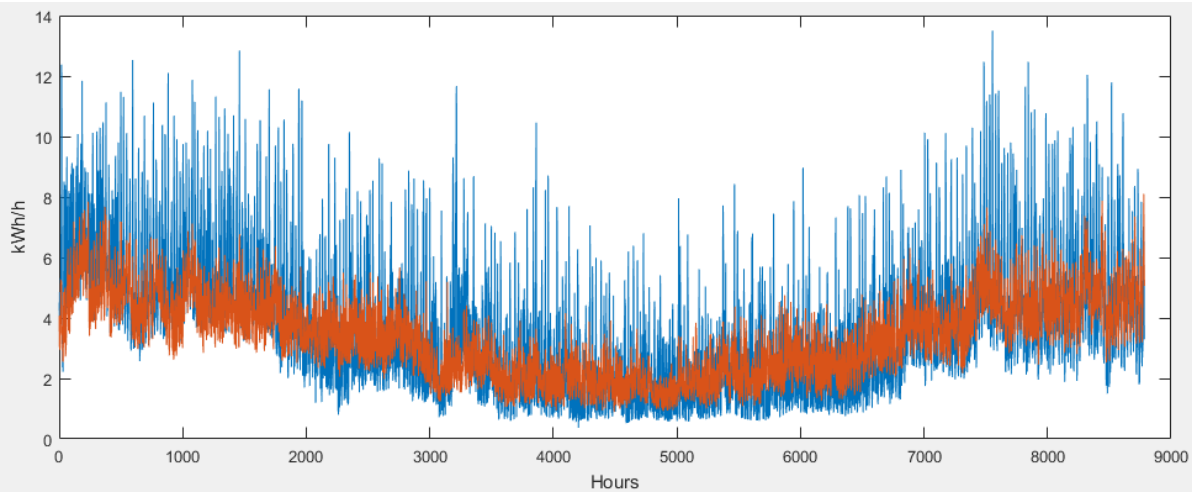

The orange graph is the average consumption of four neighbors in the same area. All of these are assumed to not possess any EVs, as their consumption graphs are flat and predictable.

The sample was chosen so that the orange graph's total energy use is just about 3000 kWh lower than the EV-owning household. These 3000 kWh are the expected EV-related consumption.

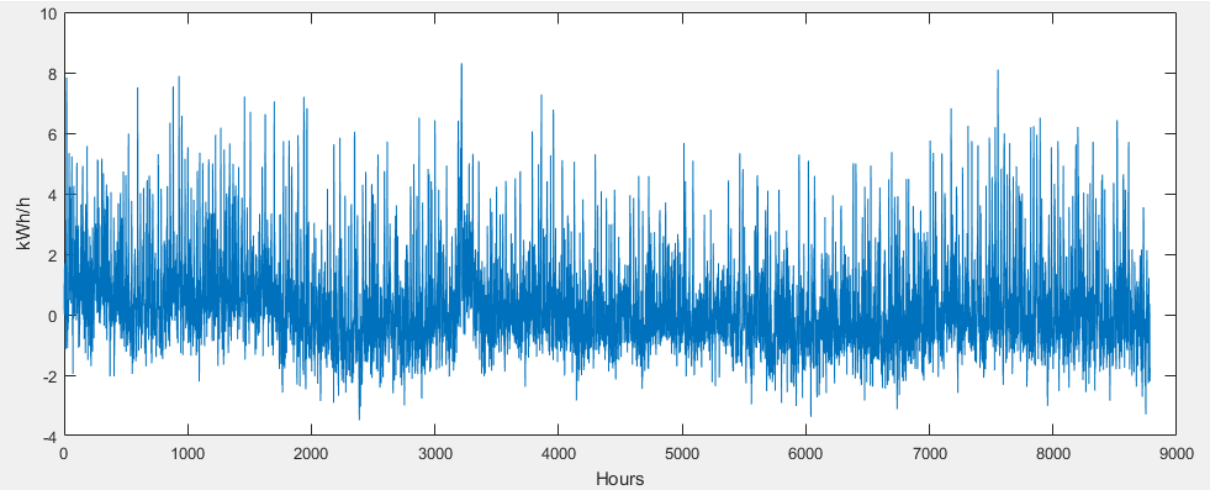

This graph is the result obtained by subtracting the orange graph from the blue one in the last picture. It oscillates around the x-axis, displaying "negative consumption" which has to be removed.

Apart from the noise, it looks somewhat promising now, with the peaks mostly staying below 7.4 kW, which is the expected maximum power consumption from a single phase 32 A charger.

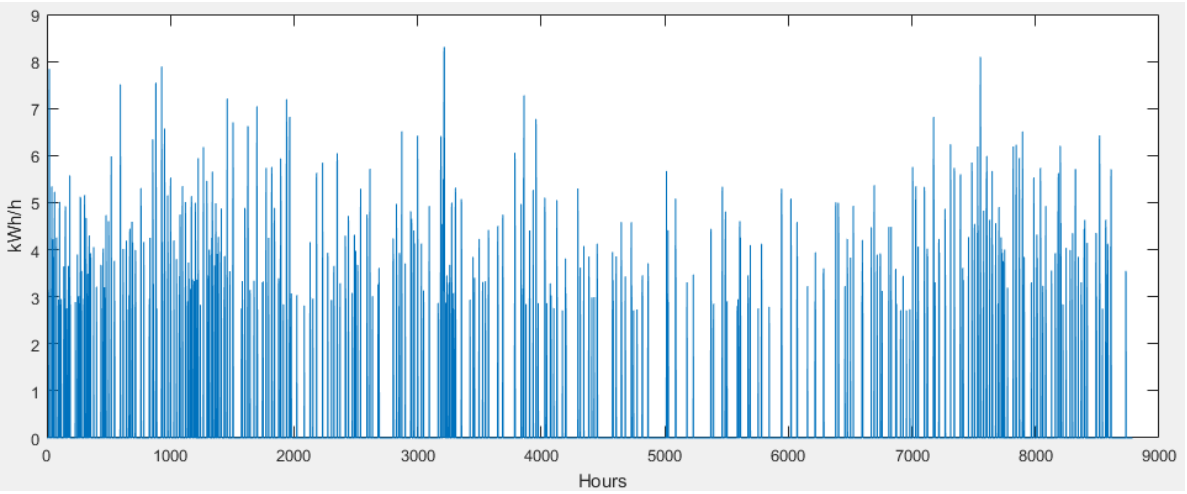

Here, all power consumption values below 2.7 kW have been set to zero. This was done in an attempt to remove the "noise" in the previous graph.

Since both positive and negative consumption values were removed, the total energy use was not noticeably changed - it is just below 3000 kWh.

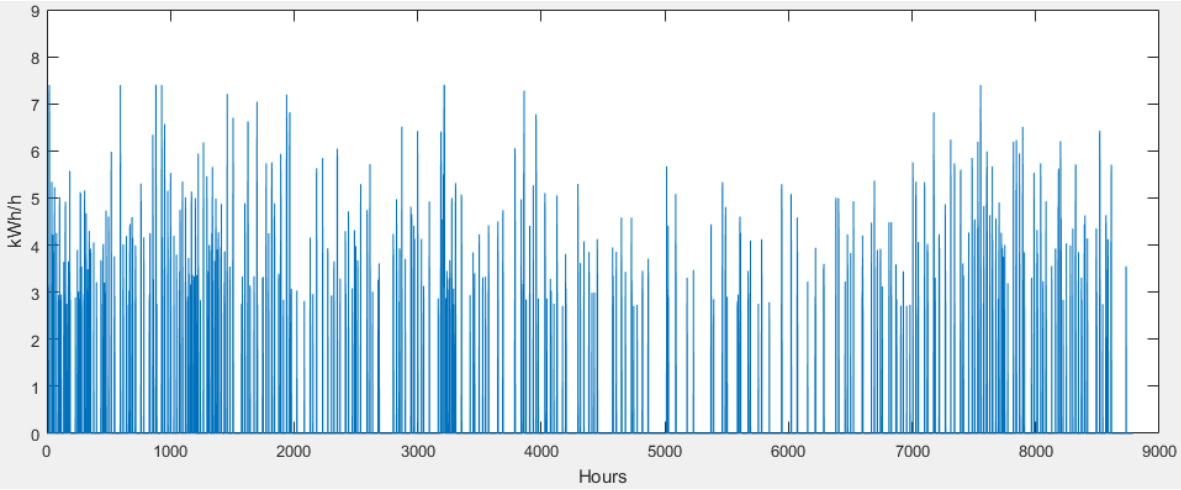

Finally, all peaks above 7,4 kW were clipped down to 7.4 kW, since it's physically impossible to draw more than that from a single phase. This is the final EV charging profile being used in this thesis.

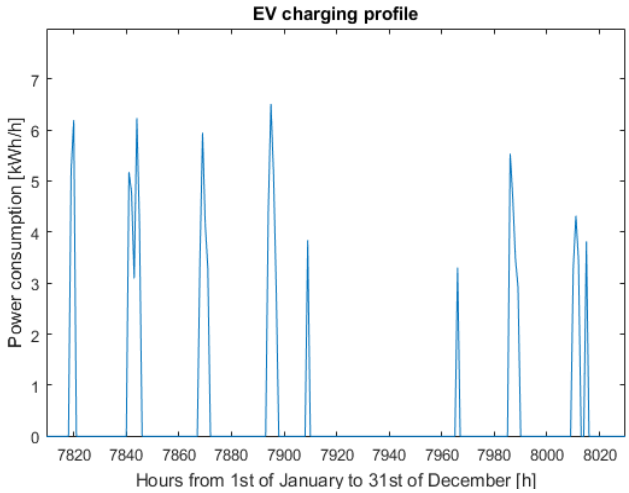

Here is an excerpt from the charging profile. The typical charging pattern tends to be a few hours every day, which usually sums up to an energy amount between 4 to 12 kWh per day.

C Table: EV loads removed

Table C.1: A list of which EV-loads were chosen to be removed for each potential fast charger location

Feeder no.	**EV-load removed at bus...**
A1	19,22,24,9,10
A2	9,28,24,22,19
B	10,12,19,22,24
C	12,19,22,24,9
D1	11,20,52,51,10
D2	11,10,51,52,20
E	20,52,51,11,46
F1	51,52,20,11,46
F2	51,52,20,46,31
G1	16,31,46,37,37
G2	40,41,35,16,31
G3	40,41,35,16,31
G4	40,41,35,16,31
H	16,31,37,37,36
I	37,37,36,39,39
J	36,37,37,39,39
K	39,39,39,36,38
L	38,38,33,39,39
M1	33,38,38,42,42
M2	42,42,42,33,38

D Location of all EVs in the 30 % EV-penetration case

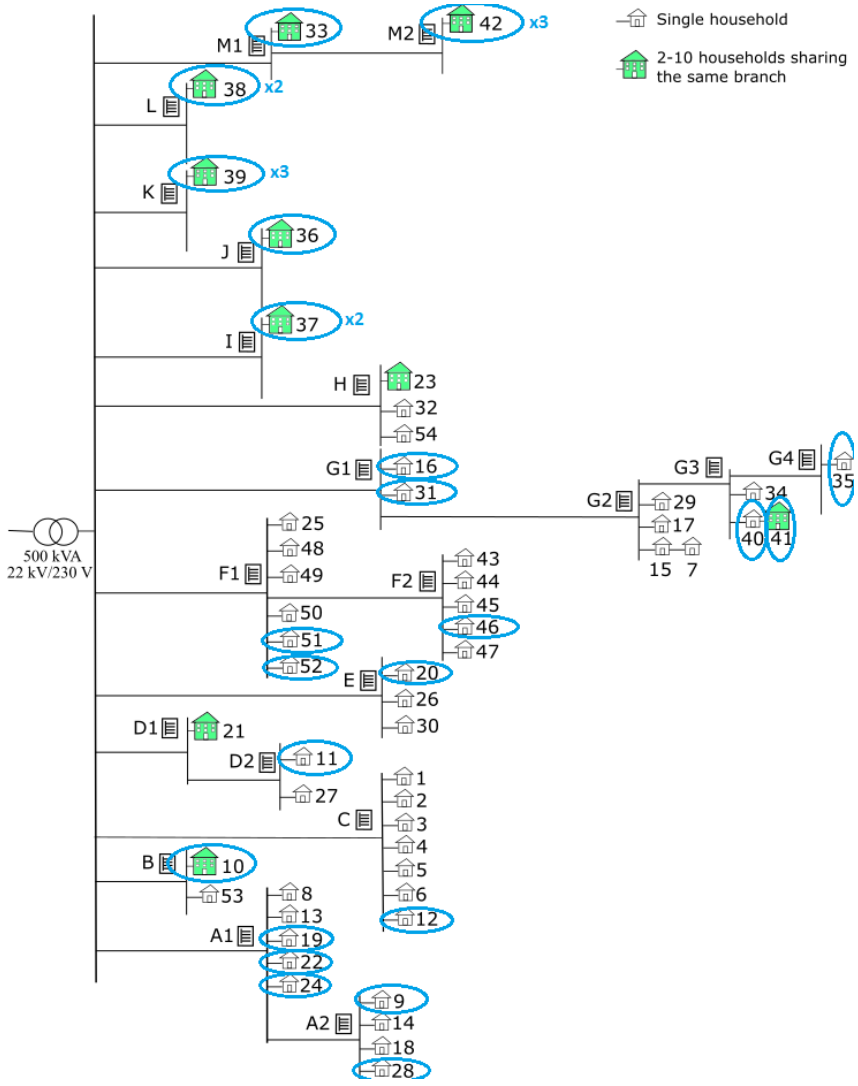

Figure D.1: Location of the 29 EVs placed the grid for the 30 % EV penetration case